
Towards Uncertainty-Aware Federated Granger Causal Learning

Ayush Mohanty*, Nazal Mohamed*, Nagi Gebraeel
Georgia Institute of Technology
Atlanta, GA 30332

Abstract

Granger causality recovers directed interactions from time-series data, but in many distributed systems, the data are vertically partitioned across clients, with each client observing only the variables of its own subsystem. Federated Granger causality (FedGC) recovers cross-client interactions without sharing raw data. Existing FedGC methods, however, return deterministic point estimates with no calibrated measure of uncertainty, leaving operators without a principled basis for identifying reliable cross-client interactions. We address this limitation by characterizing how uncertainty propagates through the FedGC framework. We derive closed-form covariance recursions for the cross-covariances induced by the coupled client-server feedback loop, and establish spectral-radius-based convergence conditions yielding closed-form expressions for the steady-state variances at both the client and server. Under mild stability conditions, we prove that the steady-state uncertainty depends only on client data statistics (aleatoric) and is independent of the priors placed on the model parameters (epistemic). Building on this asymptotic characterization, we construct a post-training hypothesis testing procedure that separates genuine cross-client interactions from spurious edges. Experiments on synthetic and real-world datasets show that the predicted uncertainty propagation matches the theory across multiple operating regimes, while consistently outperforming the state-of-the-art federated causal structure learning baselines.

1 Introduction

Complex industrial systems such as smart grids, distributed manufacturing networks, and multi-party supply chains are composed of geographically distributed subsystems that interact through tightly coupled physical and operational dependencies. The state of one subsystem depends not only on its own past but also on the past states of other subsystems, inducing a decentralized, coupled dynamical system in which these cross dependencies define a causal structure. Identifying the causal interactions among these subsystems is critical for tasks such as fault diagnosis, intervention, and risk mitigation. The key challenge is that each subsystem is operated by a different party (client), and the data needed to identify dependencies across subsystems cannot be shared due to data sovereignty constraints.

This decentralized structure corresponds to a vertical (feature-partitioned) federated learning (FL) setting (Yang et al. [2019]), where each client owns variables distinct to its own subsystem, and the cross-client couplings define the causal structure of interest. This differs sharply from the more familiar horizontal FL setting, where clients hold the same features over different observations. This distinction is consequential because cross-client interactions exist only across feature partitions and cannot be recovered by horizontal FL methods that pool gradients over a shared feature space.

*Both authors contributed equally to this work

Federated Granger causality (FedGC), recently introduced by Mohanty et al. [2025], recovers cross-client interactions without sharing raw data. Since each client only observes the variables of its own subsystem, FedGC equips it with a local model augmented by a learnable component that absorbs the unobserved influence of other clients’ variables. The server explicitly estimates cross-client interactions based on what the clients communicate. Cross-client causality is recovered through iterative updates between client augmentations and server estimates. This coupling is the structural reason why uncertainty in FedGC behaves differently from uncertainty in other FL frameworks. The randomness in client data, in local augmentation parameters, and in server estimates is all coupled through a loop, producing cross-covariances that govern how uncertainty propagates through the system. However, the existing FedGC framework returns point estimates of cross-client causal structure with no calibrated measure of how much trust to place in any individual edge, leaving operators without a defensible basis for acting on inferred influences they cannot validate locally. This gap motivates the need for a principled characterization of uncertainty in federated causal learning.

This paper develops an uncertainty-aware FedGC methodology that enables principled selection of cross-client edges. We close the gap in FedGC by characterizing how uncertainty propagates through the feedback loop, identifying the asymptotic uncertainty the trained model carries, and using that characterization to support a post-training statistical test that distinguishes genuine cross-client edges from spurious ones. One of our central findings is that the asymptotic uncertainty depends only on client data statistics. The epistemic uncertainty introduced by the randomness of the initial parameters decays as training converges, leaving aleatoric uncertainty in the data as the sole driver of steady-state behavior. As a result, the uncertainty an operator inherits from a deployed FedGC model is fully determined by the characteristics of the client data, regardless of how the system was initialized.

In this work, we establish the first theoretical foundation for analyzing uncertainties in the federated Granger causal learning framework. Specifically, we address four fundamental questions:

- **Sources:** What are the primary contributors to uncertainty in federated causal learning?
- **Propagation:** How do uncertainties compound as clients & servers iteratively update their estimates?
- **Impact:** What is the asymptotic effect of these uncertainties on the inferred causal structure?
- **Utility:** How does the asymptotic value of these uncertainties support statistically principled selection of cross-client edges in vertical federated settings?

Main Contributions: The key technical contributions of our paper are as follows:

- (1) We formalize uncertainty quantification in vertically partitioned FL of coupled dynamical systems. We explicitly distinguish *data noise* (aleatoric) from *model variability* (epistemic) effects.
- (2) We derive closed-form expressions that track uncertainty propagation through the *client-to-server* and *server-to-client* channels, as well as within-client and within-server update dynamics. This analysis identifies four previously unrecognized *cross-covariance terms* that couple data and parameter uncertainties across the FedGC architecture.
- (3) We establish spectral-radius-based convergence guarantees for the full set of covariance recursions. This yields explicit closed-form solutions for the steady-state variances at the server and client.
- (4) We prove that the resulting steady-state variances depend exclusively on the clients’ raw data statistics (aleatoric). Consequently, the asymptotic uncertainty is independent of the initial epistemic priors in the FedGC framework.
- (5) Building on the asymptotic characterization in contribution (4), we construct a post-training hypothesis test that distinguishes genuine cross-client edges from spurious ones, providing a statistically principled criterion for edge selection in vertical federated settings.
- (6) We validate the framework on synthetic and real-world datasets, showing improved recovery of cross-client causal structure compared to existing federated methods.

2 Related Work

Due to the space constraints, we provide an additional literature review of several relevant centralized techniques in Appendix A. In federated learning, uncertainty quantification has primarily been approached through Bayesian methods, including federated Bayesian neural networks Yurochkin et al. [2019], personalized inference Kotelevskii et al. [2022], Zhang et al. [2022], ensemble methods Chen and Chao [2020], and Monte Carlo dropout Park et al. [2022]. While effective in horizontally partitioned IID settings Yang et al. [2019], these approaches rely on approximate posteriors (e.g., variational inference, sampling, dropout) and often treat aleatoric and epistemic uncertainties inde-

pendently. Extensions to vertical settings, such as VertiBayes Van Daalen et al. [2024], remain static and do not capture temporal dynamics or client–server uncertainty interactions. Importantly, these methods focus on predictive performance at individual clients and do not infer any causal structure. Beyond Bayesian approaches, recursive estimation methods such as federated Kalman filtering Xing and Xia [2016], Baucas and Spachos [2023] and distributed state estimation Korres [2010], Primiadanto and Lu [2016] model uncertainty propagation but assume known system dynamics/causal structure, and therefore do not require causal modeling.

Recent works on federated causal structure learning are closest to our setting. Methods such as NOTEAR-ADMM Ng and Zhang [2022], FedPCHuang et al. [2023], FDBNL Chen et al. [2025], FedDAG Gao et al., and FedCSL Guo et al. [2024] focus on horizontally partitioned IID data, where each client observes the same set of features. Consequently, they only recover causal graphs without modeling temporal dynamics. In contrast, our setting involves vertically partitioned time-series data, where clients observe different subsets of features with interdependent dynamics. To the best of our knowledge, FedGC Mohanty et al. [2025] is the only approach that operates under this setting. However, FedGC remains limited to deterministic point estimates.

3 Preliminaries & Problem Setting

State Space Model. The underlying system is modeled as a linear time-invariant (LTI) state–space:

$$h^t = A h^{t-1} + w^t, \text{ and } y^t = C h^t + v^t \quad (1)$$

where $h^t \in \mathbb{R}^p$ are the **latent low-dimensional states** and $y^t \in \mathbb{R}^d$ are the **measured high-dimensional data** at time t with $d \gg p$. A and C are the constant state-transition and observation matrices; w^t and v^t are zero-mean i.i.d. Gaussian system and measurement noise with covariances Q and R , respectively. We make the following assumptions about the LTI state space model:

1. There are M subsystems such that $h^t = [h_1^t, \dots, h_M^t]$, $y^t = [y_1^t, \dots, y_M^t]$. Each of these subsystems is a client for our problem setting. The states are such that, $h_m^t \in \mathbb{R}^{p_m}$, and $y_m^t \in \mathbb{R}^{d_m}$ with $d_m \gg p_m$, and $\sum_{m=1}^M p_m = p$, and $\sum_{m=1}^M d_m = d$.
2. The observation matrix C is block-diagonal i.e., $C = \text{diag}(C_{11}, \dots, C_{MM})$ where each block $C_{mm} \in \mathbb{R}^{d_m \times p_m}$. The block C_{mm} is known at client m .
3. The state-transition matrix A is not block-diagonal i.e., $\exists n \neq m$ s.t., $A_{mn} \neq 0$ with $A_{mn} \in \mathbb{R}^{p_m \times p_n}$. Each client m locally estimates its diagonal block A_{mm} , while the off-diagonal blocks $A_{mn} \forall n \neq m$ are **unknown**.

Granger Causality. A time series h_n is said to *Granger-cause* another series h_m if the inclusion of past values of h_n improves the prediction of h_m . In the state-space setting, this notion is captured by the off-diagonal entries of the state-transition matrix A . For instance, in a system given by,

$$\begin{pmatrix} h_1^t \\ h_2^t \end{pmatrix} = \begin{pmatrix} A_{11} & A_{12} \\ A_{21} & A_{22} \end{pmatrix} \begin{pmatrix} h_1^{t-1} \\ h_2^{t-1} \end{pmatrix} + \begin{pmatrix} w_1^t \\ w_2^t \end{pmatrix} \quad (2)$$

the series h_2 Granger-causes h_1 precisely when $A_{12} \neq 0$. More generally, $A_{mn} \neq 0$ indicates that past values of h_n influence the future of h_m , revealing a directed causal edge from client n to m . Estimating A_{mn} in a decentralized system is the goal of the FedGC framework.

3.1 Federated Granger Causality

FedGC is a server-client framework with M different clients having **unknown interdependencies** across them. We discuss the details of the client and server models in the FedGC framework.

Client Model. Each client m models its subsystem as an LTI state–space using only the local (diagonal) blocks $A_{mm} \in \mathbb{R}^{p_m \times p_m}$ and $C_{mm} \in \mathbb{R}^{d_m \times p_m}$. A Kalman filter based “**local client model**” is used to compress the high-dimensional data (measurement) $y_t^{(m)} \in \mathbb{R}^{d_m}$ into a low-dimensional state estimate $\hat{h}_t^{(m)} \in \mathbb{R}^{p_m}$ with $d_m \gg p_m \forall m \in \{1, \dots, M\}$ such that:

$$h_{m,c}^t = A_{mm} \hat{h}_{m,c}^{t-1}, \text{ and } \hat{h}_{m,c}^t = h_{m,c}^t + K_m (y_m^t - C_{mm}(h_{m,c}^t)) \quad (3)$$

where K_m is the Kalman gain computed from $(A_{mm}, C_{mm}, Q_{mm}, R_{mm})$. The local client model (Kalman Filter) ignores cross-client dynamics A_{mn} ($n \neq m$). In order to compensate for these cross-client dynamics, the client states are *augmented* with machine learning (ML) models to obtain an “*augmented client model*” as follows:

$$\hat{h}_{m,a}^t = \hat{h}_{m,c}^t + \theta_m y_m^t, \text{ and } h_{m,a}^t = A_{mm} \hat{h}_{m,a}^t \quad (4)$$

where $\theta_m \in \mathbb{R}^{p_m \times d_m}$ is a learnable matrix that captures missing cross-client effects. The loss function $(L_m)_a$ is optimized at client m with θ_m being learned using Gradient-descent based update,

$$(L_m)_a = \|y_m^t - C_{mm} h_{m,a}^t\|, \text{ with } \theta_m^{t+1} = \theta_m^t - \eta_1 \nabla_{\theta_m^t} (L_m)_a - \eta_2 \nabla_{\theta_m^t} L_s \quad (5)$$

In Eq 5, η_1, η_2 are the learning rates corresponding to client m 's loss function $(L_m)_a$ and server model's loss function L_s respectively (the server model is discussed next).

Remark 3.1. In the gradient update equation above, while, $\nabla_{\theta_m^t} (L_m)_a$ can be computed locally at the client m , the gradient $\nabla_{\theta_m^t} L_s$ needs information from the server. However, the server cannot directly compute $\nabla_{\theta_m^t} L_s$ as the gradient is w.r.t. client model parameter θ_m . Therefore, the FedGC framework adopts chain rule to decompose it such that: $\nabla_{\theta_m^t} L_s = (\nabla_{\hat{h}_{m,a}^t} L_s) (\nabla_{\theta_m^t} \hat{h}_{m,a}^t)$. A key advantage of this decomposition is that the first factor i.e., $\nabla_{\hat{h}_{m,a}^t} L_s$ can be communicated from the server to client m , while $\nabla_{\theta_m^t} \hat{h}_{m,a}^t$ can be computed locally at client m .

Server Model. The server collects from each client m the pair $(\hat{h}_{m,c}^{t-1}, \hat{h}_{m,a}^{t-1})$ and stacks them into

$$H_c^{t-1} = [\hat{h}_{1,c}^{t-1}, \dots, \hat{h}_{M,c}^{t-1}], \text{ and } H_a^t = [A_{11} \hat{h}_{1,a}^{t-1}, \dots, A_{MM} \hat{h}_{M,a}^{t-1}] \quad (6)$$

The diagonal matrix $\text{diag}(A_{11}, \dots, A_{MM})$ estimated locally by the clients is assumed to be known at the server. However, the off-diagonal blocks (representing the GC) $A_{mn} \forall n \neq m$ are **unknown**. The server model's goal is to predict the next-step state H_s^t as follows:

$$H_s^t = [h_{1,s}^t, \dots, h_{M,s}^t] \text{ s.t., } h_{m,s}^t = A_{mm} \hat{h}_{m,c}^{t-1} + \sum_{n \neq m} \hat{A}_{mn} \hat{h}_{n,c}^{t-1}. \quad (7)$$

where the estimated causality $\hat{A}_{mn} \forall n \neq m$ are learned by minimizing the server loss function L_s with gradient-descent based updating used to learn $\hat{A}_{mn} \forall n \neq m$ with server learning rate γ s.t.,

$$L_s = \|H_a^t - H_s^t\|_2^2; \quad \hat{A}_{mn}^{t+1} = \hat{A}_{mn}^t, \text{ with } -\gamma \nabla_{\hat{A}_{mn}^t} L_s \quad (8)$$

The server then sends $\nabla_{\hat{h}_{m,a}^t} L_s$ to client m for subsequent client parameter updating.

4 Sources of Uncertainty

We partition the stochastic elements of FedGC into two disjoint sources:

(1) Aleatoric. Aleatoric uncertainty captures the irreducible noise (both measurement and process noise) ϵ_m^t in client m 's data, i.e., y_m^t . When a client updates its parameter θ_m^t via gradient descent, this data noise ϵ_m^t propagates directly into the gradient $\nabla_{\theta_m^t} (L_m)_a$ and hence into the variance of θ_m^t . Likewise, it also enters the augmented state $\hat{h}_{m,a}^t = \hat{h}_{m,c}^t + \theta_m^t y_m^t$. Since $\hat{h}_{m,a}^t$ is communicated to the server from clients, this data noise also influences the estimation of Granger causality $\hat{A}_{mn}^t \forall n \neq m$ (also called the *server model parameter*). Furthermore, this data noise affects the server loss L_s and shows up in the gradients $\nabla_{\hat{h}_{m,a}^t} L_s \forall m$ communicated from the server to the clients.

(2) Epistemic. Epistemic uncertainty reflects our lack of knowledge about the model parameters—both the client parameters θ_m and the server parameters A_{mn} . We assume both of these parameters to be **random variables** in our problem setting. Sampling from a prior $\theta_m^0 \sim \mathcal{D}_1(\mu_{\theta_m}^0, \Sigma_{\theta_m}^0)$ and $A_{mn}^0 \sim \mathcal{D}_2(\mu_{A_{mn}}^0, \Sigma_{A_{mn}}^0)$ where, \mathcal{D}_1 and \mathcal{D}_2 are any location-scale distributions, we refine θ_m^0 and \hat{A}_{mn}^0 using gradient-descent updates. By accumulating sufficient gradient-descent iterations, we reduce this epistemic uncertainty and thereby increase our confidence in the estimated causality.

Assumptions. Using these sources, we make assumptions **(A1)-(A4)** mentioned in Appendix B.

Table 1: Summary of notation (client index m , time index t)

Symbol	Meaning	Shape / Statistics
y_m^t	Raw data for client m at time t	$\in \mathbb{R}^{d_m}$; $\mu_{y_m}^t = \mathbb{E}[y_m^t]$, $\Sigma_{y_m}^t = \text{Var}(y_m^t)$
θ_m^t	Model parameter at client m	$\in \mathbb{R}^{p_m \times d_m}$
v_m^t	Vectorised θ_m^t , i.e., $v_m^t = \text{Vec}(\theta_m^t)$	$\mu_{\theta_m}^t = \mathbb{E}[v_m^t]$, $\Sigma_{\theta_m}^t = \text{Var}(v_m^t)$
Ω_m^t	Parameter-data covariance at client m	$\text{Cov}(v_m^t, y_m^t)$
Λ_m^t	Client parameter-state covariance	$\text{Cov}(v_m^t, \hat{h}_{m,a}^t)$
Ψ_{mn}^t	Server-client parameter covariance	$\text{Cov}(a_{mn}^t, v_m^t)$
Γ_{mn}^t	Cross-covariance between a_{mn}^t and $\hat{h}_{m,a}^t$	$\text{Cov}(a_{mn}^t, \hat{h}_{m,a}^t)$
$\hat{h}_{m,a}^t$	Augmented state estimate at client m	$\Sigma_{h_m}^t = \text{Var}(\hat{h}_{m,a}^t)$
\hat{A}_{mn}^t	Server parameter estimate ($n \rightarrow m$)	$\in \mathbb{R}^{p_m \times p_n}$, $\forall n \neq m$
a_{mn}^t	Vectorised \hat{A}_{mn}^t , i.e., $a_{mn}^t = \text{Vec}(\hat{A}_{mn}^t)$	$\Sigma_{A_{mn}}^t = \text{Var}(a_{mn}^t)$
L_s	Loss function at server	$\in \mathbb{R}^1$ (Scalar)
$(L_m)_a$	Loss function at client m	$\in \mathbb{R}^1$ (Scalar)
$g_{m,s}^t$	Gradient of server loss L_s w.r.t. $\hat{h}_{m,a}^t$	$\in \mathbb{R}^{p_m}$; $\text{Var}(g_{m,s}^t)$
γ	Learning rate of the server model	$\in \mathbb{R}^1$ (Scalar)
η_1, η_2	Learning rates of the client model	$\in \mathbb{R}^1$ (Scalars)

5 Uncertainty Propagation

Notation. Table 1 gives an overview of the symbols used throughout this paper.

5.1 Cross-Covariances

The FedGC framework intertwines data y_m^t , client state $\hat{h}_{m,a}^t$, client model parameter v_m^t , and server model parameter a_{mn}^t , creating four essential cross-covariances: Ω_m^t , Λ_m^t , Γ_{mn}^t and Ψ_{mn}^t , which propagates together with the individual variances. Using the notation in Table 1, Proposition 5.1 shows that v_m^t , and y_m^t are dependent with a non-zero cross-covariance Ω_m^t .

Proposition 5.1 (Client Model-Client Data Dependence). *Assume $\text{Var}(y_m^{t-1}) > 0$. Then, under the federated Granger-causality updates, $\Omega_m^t := \text{Cov}(v_m^t, y_m^t) \neq 0$.*

Using Eq 4 we know that client states $\hat{h}_{m,a}^t$ are a function of the client data y_m^t . Since $\Omega_m^t \neq 0$, there must exist a dependence between the client model and client states. Proposition 5.2 analyzes the evolution of the cross-covariance between the client parameter v_m^t , and the states $\hat{h}_{m,a}^t$.

Proposition 5.2 (Client Model-Client State Dependence). *Let $\Lambda_m^t := \text{Cov}(v_m^t, \hat{h}_{m,a}^t)$. Then we have the following recursion within the client, $\Lambda_m^t = \Sigma_{\theta_m}^t (I_{d_m} \otimes \mu_{y_m}^t) + \Omega_m^t (\mu_{v_m}^t \otimes I_{d_m})$,*

Due to the iterative communication between client and server, the client model dynamics are coupled with that of the server model in a feedback loop. Essentially, the client's noisy state estimates $\hat{h}_{m,a}^t$ affect the server estimate a_{mn}^t , and the server's uncertain a_{mn}^t in turn influences subsequent client state estimates. This effect is captured as the cross-covariance term Γ_{mn}^t given in Lemma 5.3.

Lemma 5.3 (Client State-Server Model Dependence). *The cross-covariance term $\Gamma_{mn}^t := \text{Cov}(a_{mn}^t, \hat{h}_{m,a}^t)$ follows, $\Gamma_{mn}^{t+1} = D_n^t \Gamma_{mn}^t + 2\gamma B_{mn}^t \Sigma_{h_m}^t$ where, $D_n^t := (I - 2\gamma \hat{h}_{n,c}^t \hat{h}_{n,c}^{t\top}) \otimes I$, $B_{mn}^t := \hat{h}_{n,c}^t \otimes A_{mm}$, and $\Sigma_{h_m}^t := \text{Var}(\hat{h}_{m,a}^t)$.*

Because the client parameter and its augmented state are already linked through the cross-covariance in Proposition 5.2, the client state-to-server model coupling of Lemma 5.3 propagates that link one step further, yielding a direct client model-to-server model dependence captured in Lemma 5.4.

Lemma 5.4 (Client Model-Server Model Dependence). *$\Psi_{mn}^t := \text{Cov}(a_{mn}^t, v_m^t)$ evolves as,*

$$\begin{aligned} \Psi_{mn}^{t+1} = & D_n^t \Psi_{mn}^t H_m^{t\top} + D_n^t \Gamma_{mn}^t G_m^{t\top} - D_n^t \Sigma_{A_{mn}}^t P_m^{t\top} + 2\gamma B_{mn}^t \Lambda_m^t H_m^{t\top} \\ & + 2\gamma B_{mn}^t \Sigma_{h_m}^t G_m^{t\top} - 2\gamma B_{mn}^t \Gamma_{mn}^{t\top} P_m^{t\top}, \end{aligned}$$

with the following gain matrices, $B_{mn}^t := \hat{h}_{n,c}^t \otimes A_{mm}$, $D_n^t := (I - 2\gamma \hat{h}_{n,c}^t \hat{h}_{n,c}^{t\top}) \otimes I$, $G_m^t := 2\eta_1 (y_m^t \otimes (C_{mm} A_{mm})^\top)$, $P_m^t := -2\eta_2 (y_m^t \otimes A_{mm}^\top)$, and $H_m^t := I_{p_m d_m} - 2\eta_1 (y_m^t y_m^{t\top}) \otimes ((C_{mm} A_{mm})^\top C_{mm} A_{mm}) - 2\eta_2 (y_m^t y_m^{t\top}) \otimes (A_{mm}^\top A_{mm})$

5.2 During Communication

We characterize the communication channel as the conduit through which every existing uncertainty, i.e., client-side data noise, client-parameter variance, and server-parameter variance, is redistributed at each iteration. Specifically we analyze the uncertainty propagation in both **(I) client-to-server**, and **(II) server-to-client** communication.

(I) Client to Server. At iteration t , client m sends its augmented states $\hat{h}_{m,a}^t$ to the server. While $\hat{h}_{m,a}^t$ naturally captures $\Sigma_{\theta_m}^t$ and $\Sigma_{y_m}^t$, it may also include cross-covariance $\Omega_m^t := \text{Cov}(v_m^t, y_m^t)$. Lemma 5.5 provides a closed-form for the uncertainty in $\hat{h}_{m,a}^t$ using $\Sigma_{\theta_m}^t$, $\Sigma_{y_m}^t$, and Ω_m^t .

Lemma 5.5 (Uncertainty in Client-to-Server). *Let $\kappa_m := \text{tr}(\Sigma_{y_m}^t) + \|\mu_{y_m}^t\|^2$. Then the variance in the $\hat{h}_{m,a}^t$ is, $\Sigma_{h_m}^t = \kappa_m \Sigma_{\theta_m}^t + \Omega_m^t (\mu_{y_m}^t \otimes I_{p_m})^\top + (\mu_{y_m}^t \otimes I_{p_m}) \Omega_m^{t\top}$.*

(II) Server to Client. At iteration t , the server's uncertainty is encoded in the random matrix \hat{A}_{mn}^t . Instead of sending \hat{A}_{mn}^t , the server computes and transmits the gradient: $g_{m,s}^{t+1} := \nabla_{\hat{h}_{m,a}^t} L_s^t$ where $L_s^t = \|A_{mm}[\hat{h}_{m,a}^t - \hat{h}_{m,c}^t] - \sum_{n \neq m} \hat{A}_{mn}^t \hat{h}_{n,c}^t\|^2$. This gradient inherits uncertainty from both \hat{A}_{mn}^t and $\hat{h}_{m,a}^t$, propagating the server's model uncertainty to client m . Lemma 5.6 shows that $g_{m,s}^t$ captures the uncertainty in the server parameters, client states, and their cross-covariance.

Lemma 5.6 (Uncertainty in Server-to-Client). *The uncertainty in the server communicated gradient is, $\text{Var}(g_{m,s}^{t+1}) = A_{mm}^\top U^t A_{mm}$, where, $U^t := A_{mm} \Sigma_{h_m}^t A_{mm}^\top + \sum_{n \neq m} (h_{n,c}^t h_{n,c}^{t\top}) \Sigma_{A_{mn}}^t - 2 \sum_{n \neq m} A_{mm} \Gamma_{mn}^t h_{n,c}^{t\top}$.*

5.3 Within Server

In Sections 5.1 and 5.2, we quantified how **(i)** the client-server cross-covariance Γ_{mn}^t , and **(ii)** client m 's state variance $\Sigma_{h_m}^t$ propagate during the iterative optimization of the FedGC framework. We now analyze their contribution to the propagation of the server's parameter uncertainty $\Sigma_{A_{mn}}^t$. Theorem 5.7 combines these components into a closed-form recursion for $\Sigma_{A_{mn}}^t$ within the server.

Theorem 5.7 (Uncertainty Propagation within Server). *The server param. covariance evolves as,*

$$\begin{aligned} \Sigma_{A_{mn}}^{t+1} &= D_n^t \Sigma_{A_{mn}}^t D_n^{t\top} + 4\gamma^2 (\hat{h}_{n,c}^t \otimes A_{mm}) \Sigma_{h_m}^t \times (\hat{h}_{n,c}^t \otimes A_{mm})^\top \\ &\quad + 2\gamma (D_n^t \Gamma_{mn}^t B_{mn}^{t\top} + B_{mn}^t \Gamma_{mn}^{t\top} D_n^{t\top}) \end{aligned}$$

with $D_n^t := (I - 2\gamma \hat{h}_{n,c}^t \hat{h}_{n,c}^{t\top}) \otimes I$, and $B_{mn}^t := \hat{h}_{n,c}^t \otimes A_{mm}$

5.4 Within Client

We now analyze the propagation of uncertainty of the client model parameter θ_m (or, v_m in vectorized form). Theorem 5.8 expresses the evolution of client model's variance $\Sigma_{\theta_m}^t$ in terms of the uncertainty in its states $\Sigma_{h_m}^{t-1}$, the server model $\Sigma_{A_{mn}}^{t-1}$, and those cross-covariances Ω_m^{t-1} , Γ_{mn}^{t-1} , Ψ_{mn}^{t-1} and Λ_m^{t-1} .

Theorem 5.8 (Uncertainty Propagation within Client). *The client param. covariance evolves as,*

$$\begin{aligned} \Sigma_{\theta_m}^t &= H_m^{t-1} \Sigma_{\theta_m}^{t-1} H_m^{t-1\top} + G_m^{t-1} \Sigma_{h_m}^{t-1} G_m^{t-1\top} + (X_m + X_m^\top) - \sum_{n \neq m} (Y_{mn} + Y_{mn}^\top) \\ &\quad - \sum_{n \neq m} (Z_{mn} + Z_{mn}^\top) + \sum_{n \neq m} P_m^{t-1} \Sigma_{A_{mn}}^{t-1} P_m^{t-1\top}, \end{aligned}$$

where, $X_m := H_m^{t-1} \Lambda_m^{t-1} G_m^{t-1\top}$, $Y_{mn} := H_m^{t-1} \Psi_{mn}^{t-1} P_m^{t-1\top}$, $Z_{mn} := G_m^{t-1} \Gamma_{mn}^{t-1} P_m^{t-1\top}$, $G_m^{t-1} := 2\eta_1 (y_m^{t-1} \otimes (C_{mm} A_{mm})^\top)$, $P_m^{t-1} := -2\eta_2 (y_m^{t-1} \otimes A_{mm}^\top)$, $H_m^{t-1} := I_{p_m d_m} - 2\eta_1 (y_m^{t-1} y_m^{t-1\top}) \otimes ((C_{mm} A_{mm})^\top C_{mm} A_{mm}) - 2\eta_2 (y_m^{t-1} y_m^{t-1\top}) \otimes (A_{mm}^\top A_{mm})$

6 Steady-State Impact of Uncertainty

For tractability, we assume, **(I)** $\lim_{t \rightarrow \infty} y_m^t = \mu_{y_m}$, and **(II)** $\lim_{t \rightarrow \infty} \hat{h}_{m,c}^t = \hat{h}_{m,c} \forall m$. Under these assumptions, Proposition 6.1 proves that the gains $(D_n^t, H_m^t, G_m^t, P_m^t)$ converge in the limit $t \rightarrow \infty$.

Proposition 6.1 (Gain Matrices Convergence). *The gain matrices used in Section 5 converges as, $\lim_{t \rightarrow \infty} (D_n^t, H_m^t, G_m^t, P_m^t) = (D_n, H_m, G_m, P_m)$ with, $D_n := (I - 2\gamma \hat{h}_{n,c} \hat{h}_{n,c}^\top) \otimes I$, $G_m := 2\eta_1 (\mu_{y_m} \otimes (C_{mm} A_{mm})^\top)$, $P_m := -2\eta_2 (\mu_{y_m} \otimes A_{mm}^\top)$ and $H_m := I_{p_m d_m} - 2\eta_1 (\mu_{y_m} \mu_{y_m}^\top) \otimes ((C_{mm} A_{mm})^\top C_{mm} A_{mm}) - 2\eta_2 (\mu_{y_m} \mu_{y_m}^\top) \otimes (A_{mm}^\top A_{mm})$.*

With stable gains, Proposition 6.2 shows that the cross-covariance terms Γ_{mn}^t and Ψ_{mn}^t also converge, each given in closed form. Corollary 6.3 then expresses the client-state variance $\Sigma_{h_m}^\infty$ in terms of the client-parameter variance $\Sigma_{\theta_m}^\infty$ and the data moments; no other stochastic quantity survives.

Proposition 6.2. *If $\rho(D_n), \rho(H_m) < 1$ then we have, $\lim_{t \rightarrow \infty} (\Gamma_{mn}^t, \Psi_{mn}^t) = (\Gamma_{mn}^\infty, \Psi_{mn}^\infty)$ with, $\Gamma_{mn}^\infty := (I - D_n)^{-1} 2\gamma B_{mn} \Sigma_{h_m}^\infty$, and $\Psi_{mn}^\infty := (I - H_m \otimes D_n)^{-1} \text{Vec}(D_n \Gamma_{mn}^\infty G_m^\top - D_n \Sigma_{A_{mn}}^\infty P_m^\top)$.*

Corollary 6.3. *The uncertainty in the client states converges as, $\Sigma_{h_m}^\infty = \kappa_m \Sigma_{\theta_m}^\infty + \Omega_m^\infty (\mu_{y_m} \otimes I)^\top + (\mu_{y_m} \otimes I) \Omega_m^{\infty \top}$, where $\Sigma_{h_m}^\infty := \lim_{t \rightarrow \infty} \Sigma_{h_m}^t$, $\kappa_m := \text{tr}(\Sigma_{y_m}) + \|\mu_{y_m}\|^2$ and $\Omega_m^\infty := \Sigma_{\theta_m}^\infty \mu_{y_m}$.*

The key theoretical result on the impact of uncertainty quantification is mentioned next in Theorems 6.4, and 6.5, where we show that the steady-state uncertainties of server and client models are dependent only on the client data distribution (aleatoric uncertainty), and independent of the prior distribution of the parameters (epistemic uncertainty).

We know that the steady distribution of the client m 's raw data is given by $E[y_m] = \mu_{y_m}$, and $\text{Var}(y_m) = \Sigma_{y_m}$. Using $(\mu_{y_m}, \Sigma_{y_m})$ we define the following two terms that will be used in the Theorems 6.4, and 6.5: **(I)** $M_m = \mu_{y_m} \otimes I_{p_m}$, and **(II)** $\kappa_m = \text{tr}(\Sigma_{y_m}) + \|\mu_{y_m}\|^2$

Theorem 6.4 (Convergence of Server Model's Uncertainty). *Let $\rho(D_n) < 1$. Define $\mathcal{L}_n(X) := D_n X D_n^\top$ and $Q_{mn}(\Sigma) := 4\gamma^2 B_{mn} (\kappa_m \Sigma + \Sigma M_m M_m^\top + M_m M_m^\top \Sigma) B_{mn}^\top$. Then, $\Sigma_{A_{mn}}^\infty := \lim_{t \rightarrow \infty} \Sigma_{A_{mn}}^t$ exists, is unique, and is given by, $\Sigma_{A_{mn}}^\infty = \sum_{k=0}^{\infty} \mathcal{L}_n^k(Q_{mn}(\Sigma_{\theta_m}^\infty))$*

Theorem 6.5 (Convergence of Client Model's Uncertainty). *Let $\rho(H_m) < 1$. Write $\mathcal{M}_m(\Sigma) := H_m \Sigma H_m^\top$ and $R_m(\Sigma) := G_m (\kappa_m \Sigma + \Sigma M_m M_m^\top + M_m M_m^\top \Sigma) G_m^\top$. Then the steady-state $\Sigma_{\theta_m}^\infty := \lim_{t \rightarrow \infty} \Sigma_{\theta_m}^t$ is the unique solution to $\Sigma_{\theta_m}^\infty = \mathcal{M}_m(\Sigma_{\theta_m}^\infty) + R_m(\Sigma_{\theta_m}^\infty) + P_m \Sigma_{A_{mn}}^\infty P_m^\top$.*

Theorem 6.4 shows that the steady state uncertainty of the server parameter represented by $\Sigma_{A_{mn}}^\infty$ depends only on the distribution of client data $(\mu_{y_m}, \Sigma_{y_m})$, and the steady state client model's variance $\Sigma_{\theta_m}^\infty$. It is **independent of the prior variance** $\Sigma_{A_{mn}}^0$. Similarly, Theorem 6.5 establishes that the steady-state variance of the client model $\Sigma_{\theta_m}^\infty$ is uniquely determined by the client data distribution $(\mu_{y_m}, \Sigma_{y_m})$, and the converged server uncertainty $\Sigma_{A_{mn}}^\infty$. Crucially, this result confirms that the client's epistemic uncertainty is governed entirely by aleatoric quantities and training dynamics, and is **independent of the initial variance** $\Sigma_{\theta_m}^0$.

7 Downstream Utility: Uncertainty-Aware FedGC

Building on the asymptotic covariance $\Sigma_{A_{mn}}^\infty$, in this section, we devise an approach to improve cross-client edge recovery in FedGC. Existing FedGC methods declare an edge whenever $\hat{A}_{mn} \neq 0$. However, finite-sample effects and heterogeneous noise often produce small, nonzero estimates, making it difficult to distinguish genuine interactions from spurious ones. To address this limitation, we construct a post-training hypothesis test: $H_0 : A_{mn} = 0$, and $H_1 : A_{mn} \neq 0$.

Let \hat{A}_{mn} denote the converged edge estimate, and let $\sigma_{A_{mn}}$ denote the corresponding asymptotic standard deviation obtained from $\Sigma_{A_{mn}}^\infty$. Assuming approximate normality of the converged estimator, we compute $T_{A_{mn}} = \frac{\hat{A}_{mn}}{\sigma_{A_{mn}}}$. The null hypothesis is rejected if $|T_{A_{mn}}| > t_{\nu, 1-\alpha/2}$, where $t_{\nu, 1-\alpha/2}$ denotes the Student- t critical value at significance level α with ν degrees of freedom. Equivalently, an edge is retained only if zero lies outside $\hat{A}_{mn} \pm t_{\nu, 1-\alpha/2} \sigma_{A_{mn}}$.

This yields an uncertainty-aware criterion for identifying significant cross-client interactions.

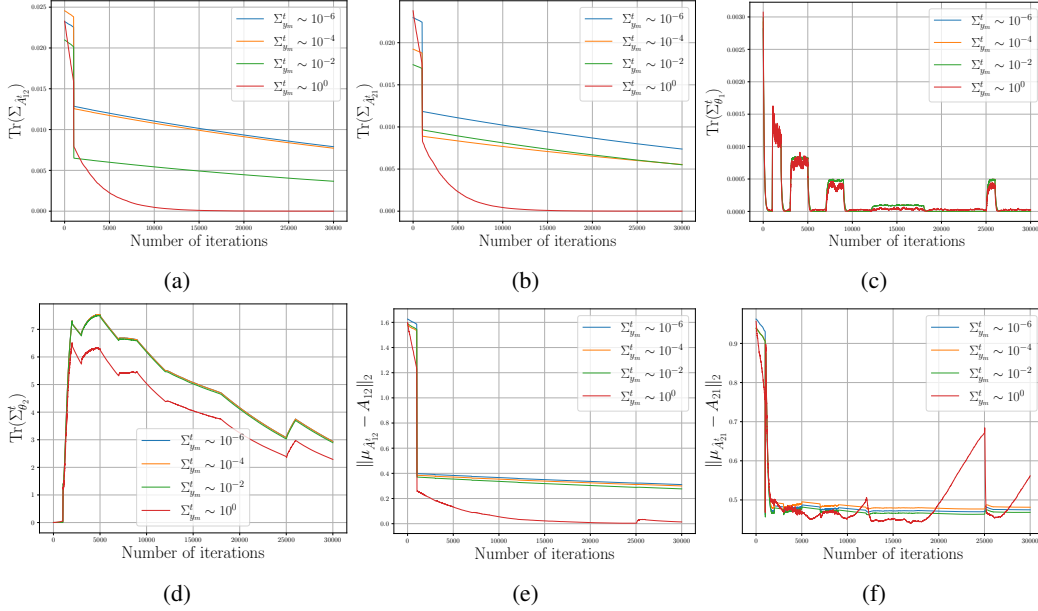


Figure 1: Uncertainty prop. during training for different levels of $\Sigma_{y_m}^t$ highlighting (a) $\text{Tr}(\Sigma_{\hat{A}_{12}}^t)$, (b) $\text{Tr}(\Sigma_{\hat{A}_{21}}^t)$, (c) $\text{Tr}(\Sigma_{\theta_1}^t)$, (d) $\text{Tr}(\Sigma_{\theta_2}^t)$, (e) $\|\mu_{\hat{A}_{12}}^t - A_{12}\|_2$, (f) $\|\mu_{\hat{A}_{21}}^t - A_{21}\|_2$ vs iter. t

8 Experiments

Synthetic Dataset. We simulate a multi-client linear time-invariant (LTI) state-space model as described in Section 3 across three experimental settings. The first set validates our theoretical results using a simple two-client setup with $p_m = 2$ and $d_m = 8$ for $m \in \{1, 2\}$, where the state matrix satisfies $A_{12} = 0$ and $A_{21} \neq 0$. For baseline comparisons, we use a six-client setup with $p_m = 2$ and $d_m = 8$ for all $m \in \{1, \dots, 6\}$. We further evaluate scalability by varying (i) the no. of clients M and (ii) the data dim. d_m in Appendix D.3. All the experimental details are provided in Appendix D.1.

Real-world Datasets. We evaluate on three industrial datasets: (1) HIL-based Augmented ICS (HAI) Shin et al. [2021], (2) Tennessee Eastman Process (TEP) Downs and Vogel [1993], and (3) Server Machine Dataset (SMD) Su et al. [2019]. Using domain-specific system structures, we partition HAI, TEP, and SMD into 3, 9, and 5 clients, respectively.

Baselines. We compare Uncertainty-Aware FedGC against five federated causal structure learning baselines: (1) FedPC Huang et al. [2023], (2) FedDAG Gao et al., (3) NOTEARS-ADMM Ng and Zhang [2022], (4) FDBNL Chen et al. [2025], and (5) vanilla FedGC Mohanty et al. [2025]. Since FedPC, FedDAG, and NOTEARS-ADMM are designed for IID data, we extend them to the time-series setting by incorporating time-lagged variables, following Pamfil et al. [2020].

Evaluation Metrics. Following the same metrics as Han et al. [2025], we report F1-score, AUC-ROC, AUC-PR, Structural Hamming Distance (SHD), False Positives (FP), and False Negatives (FN) for the synthetic dataset with known ground-truth causal structure. For the real-world datasets without a ground-truth structure, we perform root cause analysis of anomalies and report AC@k. Details on the top- k ranking for AC@k are provided in Appendix C.

8.1 Results

Validating theory. We demonstrate theoretical results of the paper on the synthetic dataset and the real-world HAI dataset. To analyze the effect of **aleatoric uncertainty**, we vary the data variance Σ_{y_m} and track the evolution of uncertainty in the server parameters ($\hat{A}_{12}^t, \hat{A}_{21}^t$) and client parameters (θ_1^t, θ_2^t). As shown in Fig. 1, the covariance traces follow the predicted dynamics and converge, validating the propagation behavior and steady-state results in Section 5 and Theorems 6.4–6.5. Higher Σ_{y_m}

accelerates variance decay but leads to increased estimation error at large values, especially during mean shifts due to violation of Assumption **(A4)** (Appendix B).

The effect of **epistemic uncertainty** is studied by varying the prior variance of \hat{A}_{mn}^0 and θ_m^0 and observing the resulting covariance evolution. As shown in Fig.4, the dynamics and steady-state covariances remain unaffected by the initial variance, confirming that uncertainty evolution is independent of epistemic priors, consistent with Theorems 6.4 and 6.5.

Appendix D.2 contains results on the evolution of the **(a)** cross-covariance, and **(b)** uncertainty in communicated terms discussed in Section 5.

Furthermore, the statistical hypothesis test in Section 7 assumes approximate normality of the causal estimates \hat{A}_{mn} . Appendix D.4 provides QQ plots validating this assumption on the synthetic dataset.

Table 2: Causal discovery performance on a synthetic dataset with A matrix dimension 12×12 .

Method	F1 \uparrow	AUC-ROC \uparrow	AUC-PR \uparrow	SHD \downarrow	FP \downarrow	FN \downarrow
FedPC	0.235	0.567	0.494	52	0	52
FedDAG	0.333	0.600	0.533	48	0	48
NOTEAR-ADMM	0.182	0.550	0.475	54	0	54
FDBNL	0.554	0.692	0.640	37	0	37
Vanilla FedGC	0.588	0.873	0.850	84	84	0
Ours (Uncertainty-Aware FedGC)	0.645	0.873	0.850	66	66	0

Causal structure learning. For the synthetic dataset with a known ground-truth structure, Table 2 compares the proposed uncertainty-aware FedGC against FedPC, FedDAG, NOTEAR-ADMM, and FDBNL, all of which exhibit substantially higher FNs since they can not model cross-client interactions. The vanilla FedGC recovers all true cross-client edges (FN = 0), but predicts nearly all candidate edges as nonzero, resulting in a large number of FPs. Our proposed approach significantly reduces FPs while preserving zero FNs, leading to improved structural recovery performance.

Root cause analysis. Since real-world datasets do not provide ground-truth causal structures, Table 3 evaluates the inferred graphs indirectly through downstream root-cause localization performance. FedDAG, NOTEAR-ADMM, and FDBNL perform poorly at tracing anomaly propagation across subsystems since they cannot recover cross-client interactions. Interestingly, FedPC achieves comparatively stronger performance on TEP despite not modeling cross-client edges, suggesting that local subsystem dynamics may partially explain anomaly propagation in some settings. In contrast, vanilla FedGC achieves substantially stronger performance across all datasets. While our proposed approach further improves performance on TEP and SMD, a slight drop on HAI requires further investigation.

Table 3: Root cause analysis performance on real-world datasets.

Method	HAI		TEP		SMD	
	AC@1 \uparrow	AC@2 \uparrow	AC@1 \uparrow	AC@2 \uparrow	AC@1 \uparrow	AC@2 \uparrow
FedPC	0.411	0.465	0.361	0.376	0.196	0.204
FedDAG	0.460	0.467	0.148	0.204	0.203	0.204
NOTEARS-ADMM	0.462	0.467	0.150	0.227	0.204	0.204
FDBNL	0.462	0.467	0.150	0.205	0.203	0.204
Vanilla FedGC	0.802	0.958	0.292	0.307	0.688	0.974
Ours	0.799	0.952	0.292	0.311	0.688	0.978

Privacy. We provide a differential privacy analysis in Appendix H. Building on that theory, we demonstrate the impact of adding Gaussian noise on asymptotic uncertainty in Appendix D.5.

Non-linear Models. Although the proposed framework is derived under a linearity assumption, Appendix J discusses extensions to certain classes of nonlinear models. We additionally provide empirical evaluations of these nonlinear extensions in Appendix E.2.

9 Limitations

This work relies on linear dynamics, independent server estimates, and asymptotic convergence of uncertainty, assumptions that may not fully hold in real-world systems. We provide a detailed discussion of these limitations in Appendix L.

References

- Marc Jayson Baucas and Petros Spachos. Federated kalman filter for secure iot-based device monitoring services. *IEEE Networking Letters*, 5(2):91–94, 2023.
- Matthew Chan, Maria Molina, and Chris Metzler. Estimating epistemic and aleatoric uncertainty with a single model. *Advances in Neural Information Processing Systems*, 37:109845–109870, 2024.
- Hong-You Chen and Wei-Lun Chao. Fedbe: Making bayesian model ensemble applicable to federated learning. *arXiv preprint arXiv:2009.01974*, 2020.
- Jianhong Chen, Ying Ma, and Xubo Yue. Federated learning of dynamic bayesian network via continuous optimization from time series data. *IEEE Transactions on Artificial Intelligence*, 2025.
- David Maxwell Chickering. Optimal structure identification with greedy search. *Journal of machine learning research*, 3(Nov):507–554, 2002.
- James J Downs and Ernest F Vogel. A plant-wide industrial process control problem. *Computers & chemical engineering*, 17(3):245–255, 1993.
- Nikita Durasov, Doruk Oner, Jonathan Donier, Hieu Le, and Pascal Fua. Enabling uncertainty estimation in iterative neural networks. *arXiv preprint arXiv:2403.16732*, 2024.
- Erdun Gao, Junjia Chen, Li Shen, Tongliang Liu, Mingming Gong, and Howard Bondell. Feddag: Federated dag structure learning. *Transactions on Machine Learning Research*.
- Jakob Gawlikowski, Cedrique Rovile Njieutcheu Tassi, Mohsin Ali, Jongseok Lee, Matthias Humt, Jianxiang Feng, Anna Kruspe, Rudolph Triebel, Peter Jung, Ribana Roscher, et al. A survey of uncertainty in deep neural networks. *Artificial Intelligence Review*, 56(Suppl 1):1513–1589, 2023.
- Xianjie Guo, Kui Yu, Lin Liu, and Jiuyong Li. Fedcsl: a scalable and accurate approach to federated causal structure learning. In *Proceedings of the AAAI Conference on Artificial Intelligence*, volume 38, pages 12235–12243, 2024.
- Xiao Han, Saima Absar, Lu Zhang, and Shuhan Yuan. Root cause analysis of anomalies in multivariate time series through granger causal discovery. In *The Thirteenth International Conference on Learning Representations*, 2025.
- Paul Hofman, Yusuf Sale, and Eyke Hüllermeier. Quantifying aleatoric and epistemic uncertainty: A credal approach. In *ICML 2024 Workshop on Structured Probabilistic Inference & Generative Modeling*, 2024.
- Patrik Hoyer, Dominik Janzing, Joris M Mooij, Jonas Peters, and Bernhard Schölkopf. Nonlinear causal discovery with additive noise models. *Advances in neural information processing systems*, 21, 2008.
- Jianli Huang, Xianjie Guo, Kui Yu, Fuyuan Cao, and Jiye Liang. Towards privacy-aware causal structure learning in federated setting. *IEEE Transactions on Big Data*, 9(6):1525–1535, 2023.
- Eyke Hüllermeier and Willem Waegeman. Aleatoric and epistemic uncertainty in machine learning: An introduction to concepts and methods. *Machine learning*, 110(3):457–506, 2021.
- Denis Huseljic, Bernhard Sick, Marek Herde, and Daniel Kottke. Separation of aleatoric and epistemic uncertainty in deterministic deep neural networks. In *2020 25th International Conference on Pattern Recognition (ICPR)*, pages 9172–9179. IEEE, 2021.
- Aapo Hyvärinen, Kun Zhang, Shohei Shimizu, and Patrik O Hoyer. Estimation of a structural vector autoregression model using non-gaussianity. *Journal of Machine Learning Research*, 11(5), 2010.

- Azam Ikram, Sarthak Chakraborty, Subrata Mitra, Shiv Saini, Saurabh Bagchi, and Murat Kocaoglu. Root cause analysis of failures in microservices through causal discovery. *Advances in Neural Information Processing Systems*, 35:31158–31170, 2022.
- George N Korres. A distributed multiarea state estimation. *IEEE Transactions on Power Systems*, 26(1):73–84, 2010.
- Nikita Kotelevskii, Maxime Vono, Alain Durmus, and Eric Moulines. Fedpop: A bayesian approach for personalised federated learning. *Advances in Neural Information Processing Systems*, 35: 8687–8701, 2022.
- Mingjie Li, Zeyan Li, Kanglin Yin, Xiaohui Nie, Wenchi Zhang, Kaixin Sui, and Dan Pei. Causal inference-based root cause analysis for online service systems with intervention recognition. In *Proceedings of the 28th ACM SIGKDD conference on knowledge discovery and data mining*, pages 3230–3240, 2022.
- Nis Meinert, Jakob Gawlikowski, and Alexander Lavin. The unreasonable effectiveness of deep evidential regression. In *Proceedings of the AAAI Conference on Artificial Intelligence*, volume 37, pages 9134–9142, 2023.
- Yuan Meng, Shenglin Zhang, Yongqian Sun, Ruru Zhang, Zhilong Hu, Yiyin Zhang, Chenyang Jia, Zhaogang Wang, and Dan Pei. Localizing failure root causes in a microservice through causality inference. In *2020 IEEE/ACM 28th International Symposium on Quality of Service (IWQoS)*, pages 1–10. IEEE, 2020.
- Ayush Mohanty, Nazal Mohamed, Paritosh Ramanan, and Nagi Gebrael. Federated granger causality learning for interdependent clients with state space representation. *International conference on learning representations*, 2025.
- Ignavier Ng and Kun Zhang. Towards federated bayesian network structure learning with continuous optimization. In *International conference on artificial intelligence and statistics*, pages 8095–8111. PMLR, 2022.
- Roxana Pamfil, Nisara Sriwattanaworachai, Shaan Desai, Philip Pilgerstorfer, Konstantinos Georgatzis, Paul Beaumont, and Bryon Aragam. Dynotears: Structure learning from time-series data. In *International conference on artificial intelligence and statistics*, pages 1595–1605. Pmlr, 2020.
- Junha Park, Jiseon Moon, Taekyoon Kim, Peng Wu, Tales Imbiriba, Pau Closas, and Sunwoo Kim. Federated learning for indoor localization via model reliability with dropout. *IEEE Communications Letters*, 26(7):1553–1557, 2022.
- Anggoro Primadianto and Chan-Nan Lu. A review on distribution system state estimation. *IEEE Transactions on Power Systems*, 32(5):3875–3883, 2016.
- Jakob Runge. Discovering contemporaneous and lagged causal relations in autocorrelated nonlinear time series datasets. In *Conference on uncertainty in artificial intelligence*, pages 1388–1397. Pmlr, 2020.
- Jakob Runge, Peer Nowack, Marlene Kretschmer, Seth Flaxman, and Dino Sejdinovic. Detecting and quantifying causal associations in large nonlinear time series datasets. *Science advances*, 5(11):eaau4996, 2019.
- Shohei Shimizu, Patrik O Hoyer, Aapo Hyvärinen, Antti Kerminen, and Michael Jordan. A linear non-gaussian acyclic model for causal discovery. *Journal of Machine Learning Research*, 7(10), 2006.
- Hyeok-Ki Shin, Woomyo Lee, Jeong-Han Yun, and Byung-Gi Min. Two ics security datasets and anomaly detection contest on the hil-based augmented ics testbed. In *Cyber Security Experimentation and Test Workshop, CSET ’21*, page 36–40, New York, NY, USA, 2021. Association for Computing Machinery. ISBN 9781450390651. doi: 10.1145/3474718.3474719. URL <https://doi.org/10.1145/3474718.3474719>.
- Peter Spirtes and Clark Glymour. An algorithm for fast recovery of sparse causal graphs. *Social science computer review*, 9(1):62–72, 1991.

- Peter Spirtes, Clark N Glymour, and Richard Scheines. *Causation, prediction, and search*. MIT press, 2000.
- Ya Su, Youjian Zhao, Chenhao Niu, Rong Liu, Wei Sun, and Dan Pei. Robust anomaly detection for multivariate time series through stochastic recurrent neural network. In *Proceedings of the 25th ACM SIGKDD international conference on knowledge discovery & data mining*, pages 2828–2837, 2019.
- Florian Van Daalen, Lianne Ippel, Andre Dekker, and Inigo Bermejo. Vertibayes: learning bayesian network parameters from vertically partitioned data with missing values. *Complex & Intelligent Systems*, 10(4):5317–5329, 2024.
- Hanjing Wang, Dhiraj Joshi, Shiqiang Wang, and Qiang Ji. Gradient-based uncertainty attribution for explainable bayesian deep learning. In *Proceedings of the IEEE/CVF Conference on Computer Vision and Pattern Recognition*, pages 12044–12053, 2023.
- Ping Wang, Jingmin Xu, Meng Ma, Weilan Lin, Disheng Pan, Yuan Wang, and Pengfei Chen. Cloudranger: Root cause identification for cloud native systems. In *2018 18th IEEE/ACM International Symposium on Cluster, Cloud and Grid Computing (CCGRID)*, pages 492–502. IEEE, 2018.
- Zirui Xing and Yuanqing Xia. Distributed federated kalman filter fusion over multi-sensor unreliable networked systems. *IEEE Transactions on Circuits and Systems I: Regular Papers*, 63(10): 1714–1725, 2016.
- Qiang Yang, Yang Liu, Tianjian Chen, and Yongxin Tong. Federated machine learning: Concept and applications. *ACM Transactions on Intelligent Systems and Technology (TIST)*, 10(2):1–19, 2019.
- Guangba Yu, Pengfei Chen, Hongyang Chen, Zijie Guan, Zicheng Huang, Linxiao Jing, Tianjun Weng, Xinmeng Sun, and Xiaoyun Li. Microrank: End-to-end latency issue localization with extended spectrum analysis in microservice environments. In *Proceedings of the Web Conference 2021*, pages 3087–3098, 2021.
- Mikhail Yurochkin, Mayank Agarwal, Soumya Ghosh, Kristjan Greenewald, Nghia Hoang, and Yasaman Khazaeni. Bayesian nonparametric federated learning of neural networks. In *International conference on machine learning*, pages 7252–7261. PMLR, 2019.
- Xu Zhang, Yinchuan Li, Wenpeng Li, Kaiyang Guo, and Yunfeng Shao. Personalized federated learning via variational bayesian inference. In *International Conference on Machine Learning*, pages 26293–26310. PMLR, 2022.
- Xun Zheng, Bryon Aragam, Pradeep K Ravikumar, and Eric P Xing. Dags with no tears: Continuous optimization for structure learning. *Advances in neural information processing systems*, 31, 2018.

Appendix

A Additional Literature Review

Uncertainty Propagation. In centralized settings, uncertainty propagation under gradient-based optimization has been studied extensively. Prior work analyzes how stochastic gradient noise and perturbations propagate through iterative updates Wang et al. [2023], Durasov et al. [2024], Gawlikowski et al. [2023], and formalizes the interaction between aleatoric and epistemic uncertainties Chan et al. [2024], Huseljic et al. [2021], Meinert et al. [2023], Hofman et al. [2024], Hüllermeier and Waegeman [2021]. However, these analyses assume centralized access to data and do not extend to federated settings with decentralized data and client–server interactions.

Causal Structure Learning. The field of *causal structure learning* seeks to recover an adjacency graph that governs dependencies among variables in observational data. Classical approaches include constraint-based Spirtes and Glymour [1991], Spirtes et al. [2000], score-based Zheng et al. [2018], Chickering [2002], and functional model-based methods Hoyer et al. [2008], Shimizu et al. [2006], which infer directed acyclic graphs (DAGs) from fully observed datasets with IID samples. While time-series extensions for some of these methods have been proposed by Pamfil et al. [2020], Runge et al. [2019], Runge [2020], and Hyvärinen et al. [2010], all of these methods assume centralized access to data.

Root Cause Analysis. Another closely related field is *root cause analysis* (RCA) in time-series data. Representative methods include MicroCause Meng et al. [2020], MicroRank Yu et al. [2021], CloudRanger Wang et al. [2018] CIRCA Li et al. [2022], AERCA Han et al. [2025], and RCD Ikram et al. [2022], which typically combine anomaly detection with downstream root cause identification. While these methods provide practical metrics for evaluating causal interpretability in nonlinear datasets especially in scenarios where no ground-truth adjacency graph is available, they operate only in fully centralized settings.

B Assumptions

(A1) Stochasticity. For every client m , the *client model parameter* θ_m^t , and *client data* y_m^t are random variables. The local client state $\hat{h}_{m,c}^t$ is deterministic. Consequently, the only randomness entering the augmented states $\hat{h}_{m,a}^t = \hat{h}_{m,c}^t + \theta_m^t y_m^t$ comes from θ_m^t and y_m^t . In the server model, the Granger causal estimation $\hat{A}_{mn}^t \forall n \neq m$ (also called the *server model parameter*) is random.

(A2) Model Parameters. The server parameters $A_{mn}^t, n \neq m$, are mutually independent across block-rows and times. As a consequence, for any distinct clients $m \neq n$, the induced parameters θ_m^t and θ_n^t have zero cross-covariance at every time t , i.e. $\text{Cov}(\theta_m^t, \theta_n^t) = 0, \forall m \neq n, \forall t$. We formally establish this result in Lemma G.1, and Proposition G.2.

(A3) Prior. The initial server and client parameters are independent, i.e., $\hat{A}_{mn}^0 \perp\!\!\!\perp \theta_m^0$, and the initial client parameters are uncorrelated, i.e., $\text{Cov}(\theta_m^0, \theta_n^0) = 0 \forall n \neq m$.

(A4) Stationarity. Client data are weakly stationary with time-invariant first and second moments: $\mathbb{E}[y_m^t] = \mu_{y_m}, \text{Var}(y_m^t) = \Sigma_{y_m}, \forall t$

- Assumption **(A4)** is required only for the training data used in uncertainty propagation analysis and steady-state characterization. The testing data used in downstream evaluation need not satisfy weak stationarity.
- We additionally discuss relaxations of Assumption **(A4)** in Appendix J.2.

C Root Cause Analysis Metric

For real-world datasets, we evaluate the inferred causal graph using a top- k root cause analysis (RCA) metric. The objective is to determine whether the true root-cause subsystem is ranked among the top anomalous candidates identified using the learned cross-client causal structure.

For each client m , let $x_m(t) \in \mathbb{R}^2$ denote the local latent state after preprocessing. We first compute the training mean

$$\mu_m = \frac{1}{T_{\text{train}}} \sum_{t=1}^{T_{\text{train}}} x_m(t), \quad (9)$$

and the corresponding deviation norm

$$d_m(t) = \|x_m(t) - \mu_m\|_2. \quad (10)$$

The anomaly threshold for each client is then defined as the empirical 99th percentile of the training deviation norms:

$$\tau_m = Q_{0.99} \left(\{d_m(t)\}_{t=1}^{T_{\text{train}}} \right). \quad (11)$$

For each anomaly instance q , we compute a local anomaly indicator:

$$z_m^{(q)} = \mathbf{1} \left(d_m^{(q)} > \tau_m \right). \quad (12)$$

Using the pruned causal graph \hat{A} , we then compute a root-cause score for each client:

$$s_j^{(q)} = \sum_{i=1}^N z_i^{(q)} z_j^{(q)} \|A_{mn}\|_F, \quad (13)$$

where $\|A_{mn}\|_F$ denotes the Frobenius norm of the inferred cross-client interaction. Clients are subsequently ranked according to $s_j^{(q)}$.

A prediction is considered correct if the true root-cause client appears within the top- k ranked candidates. The resulting top- k accuracy metric is computed as

$$\text{AC@k} = \frac{1}{Q} \sum_{q=1}^Q \mathbf{1} (\text{true root cause} \in \text{Top-}k), \quad (14)$$

where Q denotes the total number of anomaly instances.

D Additional Results on Synthetic Dataset

D.1 Experimental Details

Experiments on a synthetic dataset were conducted by simulating a two-client LTI system. Each client has a hidden latent state dimension $p_m = 2$ and a measurement dimension $d_m = 8$. A one-way dependency in which client 1 Granger causes client 2 (and not vice-versa) is considered. Therefore $A_{12} = 0$ and $A_{21} \neq 0$. The loss functions in (5) and (8) are regularized and the learning rates γ , η_1 and η_2 are adjusted to ensure convergence but not optimally tuned.

All the results reported are in terms of the trace of the covariance matrices. Trace of the covariance matrix was chosen as a scalar quantity to quantify the uncertainty from the covariance matrices for a multitude of reasons such as: 1) it is the sum of variances across all directions, 2) it is rotation invariant, 3) computationally cheap etc. Unless otherwise specified, the quantities plotted are relevant to explaining the uncertainty propagation in learning \hat{A}_{21} .

The effect of aleatoric noise in all the experiments is studied by changing the data variance $\Sigma_{y_m}^t$, and the effect of epistemic noise is studied by changing the variance of the initial values $\Sigma_{\hat{A}_{mn}}^0$ and $\Sigma_{\theta_m}^t$.

D.2 Cross-Covariance and Communicated Terms

Cross-Covariances. The evolution of cross-covariance terms Λ_m^t , Γ_{mn}^t and Ψ_{mn}^t discussed in Section 6 for different regimes of aleatoric and epistemic noise are given in Figures 5, 6 and 7. We can observe that the cross-covariance terms converge even for very high noise regimes.

During Communication. The augmented client state $\hat{h}_{m,a}^t$ sent from the client carries the uncertainty from the client to the server and the gradient $\nabla_{\hat{h}_{m,a}^t} L_s^t$ sent back to the client carries the uncertainty from the server to the client. The evolution of covariances of these communicated terms for different aleatoric and epistemic noises is plotted in Figures 8, 9 and 10.

D.3 Scalability Studies

In the scalability experiment, we consider the two-client system with similar causal relationship as in previous experiments. The hidden state dimension $p_m = 2$ is kept constant while the measurement dimension d_m is increased for both clients. Trace of covariance of \hat{A}_{21} at convergence for regimes of $\Sigma_{\hat{A}_{mn}}^0 \sim \{10^{-6}, 10^{-4}, 10^{-2}, 10^0\}$ is summarized in Table 4. We could observe that the performance of the framework remains more or less similar with increased dimension of the measurements d_m . In the second experiment, we keep $p_m = 2$ and $d_m = 8$ and vary the number of clients M . We report the trace of covariance of \hat{A}_{21} at convergence for different regimes of $\Sigma_{\hat{A}_{mn}}^0$ in Table 5.

Table 4: Trace(Cov(\hat{A}_{21})) vs measurement (i.e., raw data) dim. d_m

Order of Variance	Measurement (Raw Data) Dimension (d_m)			
	$d_m = 16$	$d_m = 32$	$d_m = 64$	$d_m = 128$
$\sim 10^{-6}$	$\approx 10^{-9}$	$\approx 10^{-5}$	$\approx 10^{-7}$	$\approx 10^{-7}$
$\sim 10^{-4}$	$\approx 10^{-8}$	$\approx 10^{-5}$	$\approx 10^{-7}$	$\approx 10^{-7}$
$\sim 10^{-2}$	1.0×10^{-4}	4.0×10^{-4}	1.0×10^{-4}	$\approx 10^{-5}$
$\sim 10^0$	1.6722	1.9733	2.4601	1.5882

Table 5: Trace(Cov(\hat{A}_{21})) vs. no. of clients M

Order of Variance	Number of Clients (M)			
	$M = 2$	$M = 4$	$M = 8$	$M = 16$
$\sim 10^{-6}$	$\approx 10^{-5}$	$\approx 10^{-5}$	$\approx 10^{-5}$	$\approx 10^{-6}$
$\sim 10^{-4}$	$\approx 10^{-5}$	$\approx 10^{-5}$	$\approx 10^{-5}$	$\approx 10^{-6}$
$\sim 10^{-2}$	0.0001	0.0002	0.0002	0
$\sim 10^0$	1.7233	1.6456	2.5835	4.7

D.4 QQ Plots for Causal Estimates

The post-training statistical hypothesis test proposed in Section 7 assumes approximate normality of the converged causal estimates \hat{A}_{mn} . To validate this assumption empirically, Fig. 2 presents QQ plots for all entries of four randomly selected off-diagonal blocks of the estimated causal matrix on the synthetic dataset. For each selected block \hat{A}_{mn} , we generate 30 bootstrap resamples of the dataset and collect the corresponding converged causal estimates. We then compare their empirical quantiles against the theoretical quantiles of a Gaussian distribution. As shown in Fig. 2, the empirical quantiles closely follow the theoretical Gaussian quantiles across most of the distribution, indicating that the converged causal estimates are approximately normal.

D.5 Effect of DP Noise on Uncertainty and Causal Accuracy

In this subsection, we study how differentially private (DP) Gaussian noise injected into the federated messages affects (i) steady-state parameter uncertainty and (ii) accuracy of causal link detection. We consider two communication directions: *client*→*server*, where noise is added to the states sent by the clients to the server, and *server*→*client*, where noise is added to the gradients sent back to the clients. In both cases, we use the Gaussian mechanism and sweep the noise standard deviation over a log-scale grid $\sigma \in \{10^{-6}, 10^{-5}, \dots, 10^{-1}\}$.

Figure 3 summarizes the results on the synthetic dataset. The top row shows the steady-state uncertainty of the cross-client Granger block A_{21} , measured via $\text{tr}(\Sigma_{A_{21}})$, as a function of the injected noise scale σ . The bottom row reports the corresponding causal estimation accuracy, measured by the Frobenius norm $\|\hat{A}_{21} - A_{21, \text{true}}\|_F$ and normalized for visualization. Panels labelled “server→client” and “client→server” correspond to the direction in which DP noise is added. Across all configurations, the uncertainty recursions remain numerically stable for the entire range of σ , and the steady-state variance increases smoothly as the DP noise level grows. For small to moderate noise ($\sigma \sim 10^{-3}$), the inflation in $\text{tr}(\Sigma_{A_{21}})$ is modest and the causal estimation error remains close to the non-DP baseline in both communication directions. Only for the largest noise levels ($\sigma \approx 10^{-2}$ – 10^{-1}) do we

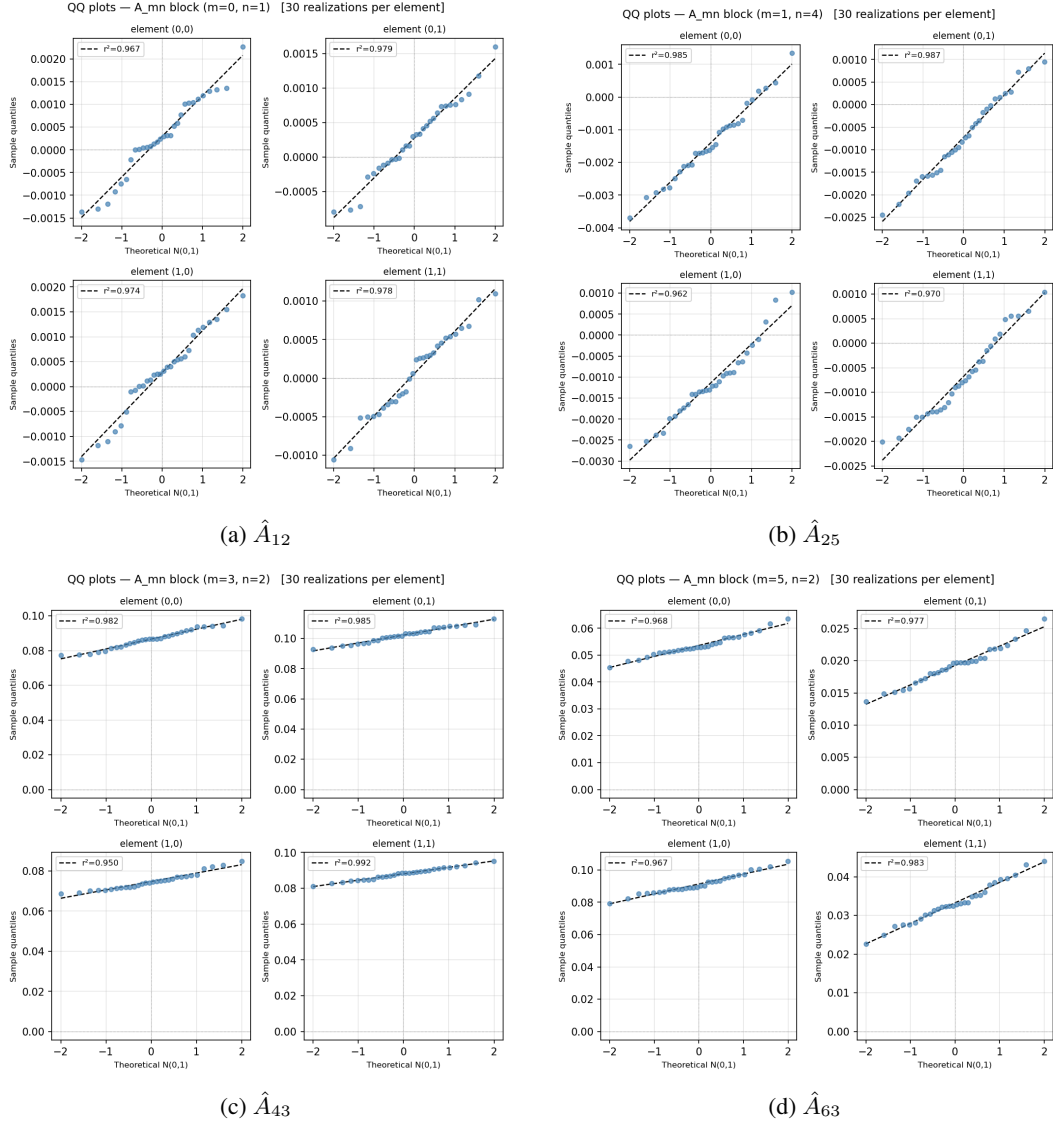


Figure 2: QQ plots for the causal estimates \hat{A}_{mn} on the synthetic dataset.

observe a pronounced increase in variance accompanied by a degradation in causal link detection, as expected from strong DP perturbations. These experiments confirm that our uncertainty propagation framework is robust to reasonably strong DP noise and that the empirical privacy–utility trade-off behaves consistently with the Gaussian mechanism in both communication channels.

E Additional Results on Real-World Dataset

E.1 Preprocessing of Real-world Datasets

For the real-world datasets, each client contains a multivariate observation stream $\mathbf{Y}^{(c)} \in \mathbb{R}^{T \times p_c}$. We first standardize each client independently using training statistics: $\tilde{\mathbf{Y}}^{(c)} = \left(\mathbf{Y}^{(c)} - \boldsymbol{\mu}_Y^{(c)} \right) \oslash \boldsymbol{\sigma}_Y^{(c)}$. Next, we compute a client-wise singular value decomposition (SVD), $\tilde{\mathbf{Y}}_{\text{train}}^{(c)} = \mathbf{U}^{(c)} \boldsymbol{\Sigma}^{(c)} \mathbf{V}^{(c)\top}$, and retain the two right singular vectors associated with the largest singular values: $\mathbf{B}^{(c)} = [\mathbf{v}_1^{(c)}, \mathbf{v}_2^{(c)}]$.

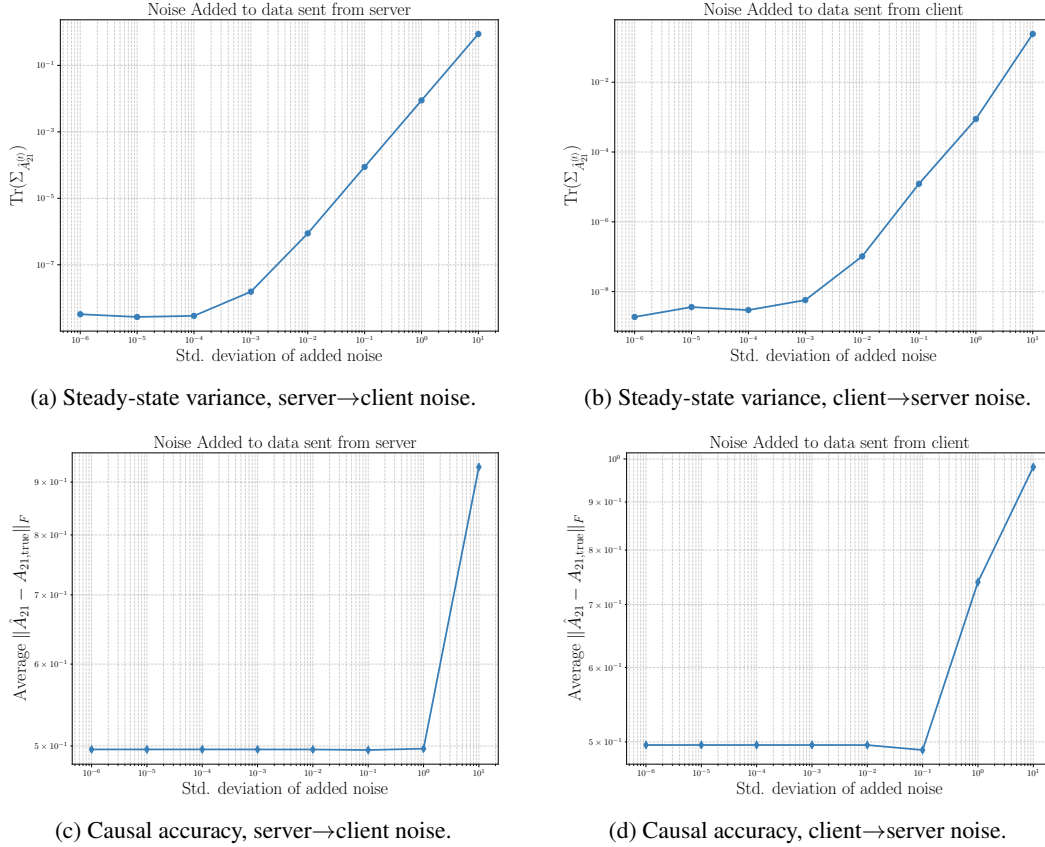


Figure 3: Effect of DP Gaussian noise on steady-state uncertainty and causal link detection in the synthetic dataset. Top row: trace of the propagated covariance $\text{tr}(\Sigma_{A_{21}})$ as a function of the noise scale σ . Bottom row: Frobenius error $\|\hat{A}_{21} - A_{21,\text{true}}\|_F$ versus σ .

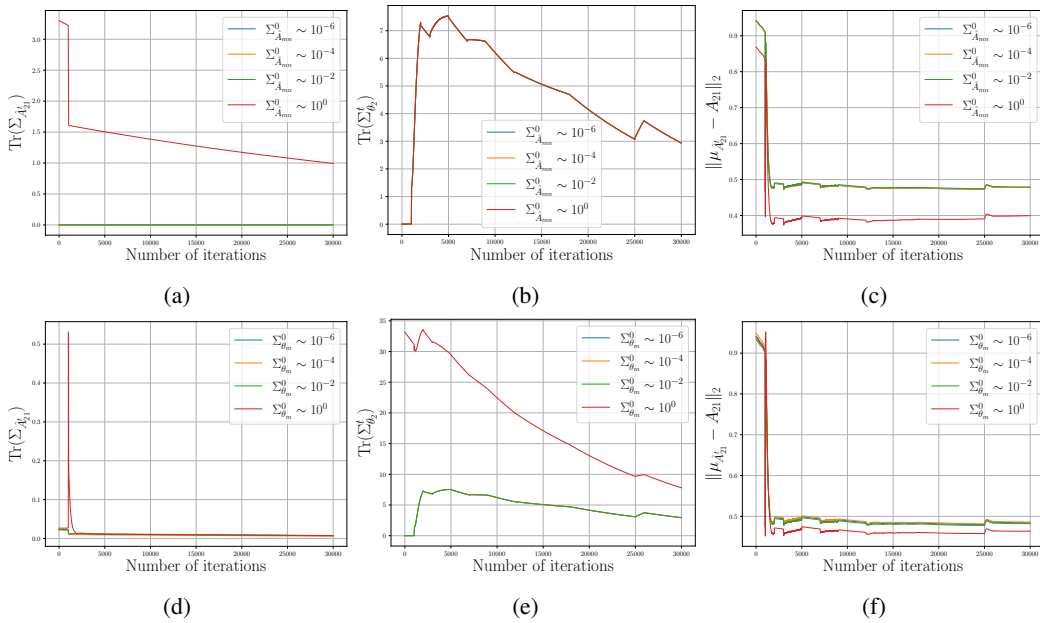


Figure 4: Uncertainty prop. highlighting (a) $\text{Tr}(\Sigma_{\hat{A}_{21}}^t)$, (b) $\text{Tr}(\Sigma_{\theta_2}^t)$, (c) $\|\mu_{\hat{A}_{21}} - A_{21}\|_2$ vs iter. t for different levels of $\Sigma_{\hat{A}_{mn}}^0$ (top row), and $\Sigma_{\theta_m}^0$ (bottom row)

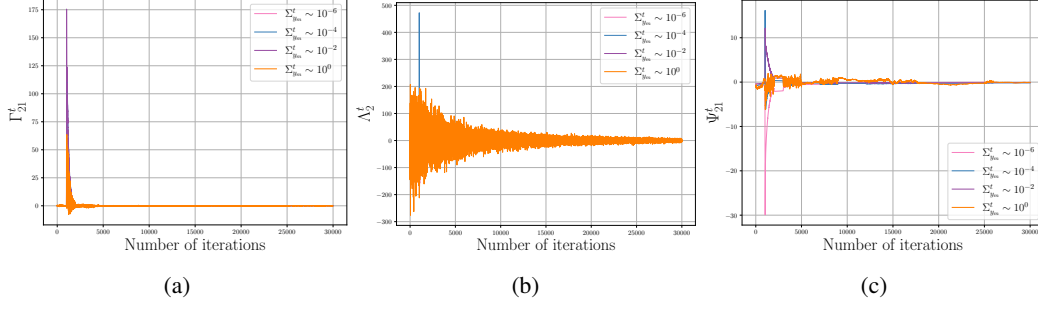


Figure 5: Uncertainty propagation in the cross-covariance terms during FedGC learning for different regimes of $\Sigma_{y_m}^t$ (a) Γ_{21}^t vs iterations, (b) Λ_2^t vs iterations, (c) Ψ_{21}^t vs iterations.in the synthetic dataset

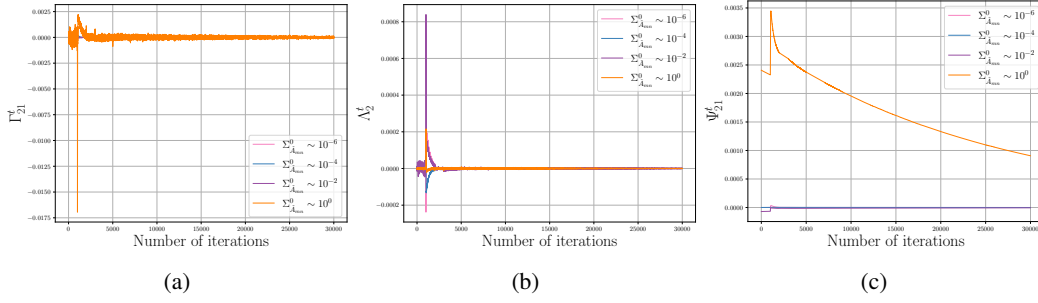


Figure 6: Uncertainty propagation in the cross-covariance terms during FedGC learning for different regimes of $\Sigma_{\hat{A}_{mn}}^0$ (a) Γ_{21}^t vs iterations, (b) Λ_2^t vs iterations, (c) Ψ_{21}^t vs iterations.in the synthetic dataset

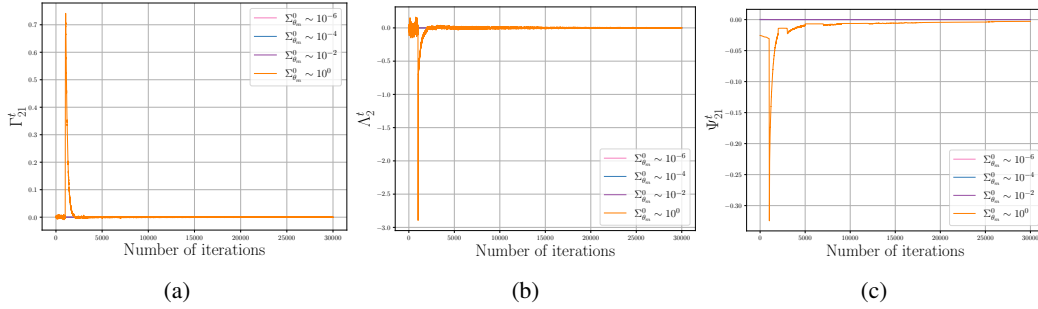


Figure 7: Uncertainty propagation in the cross-covariance terms during FedGC learning for different regimes of $\Sigma_{\theta_m}^t$ (a) Γ_{21}^t vs iterations, (b) Λ_2^t vs iterations, (c) Ψ_{21}^t vs iterations.in the synthetic dataset

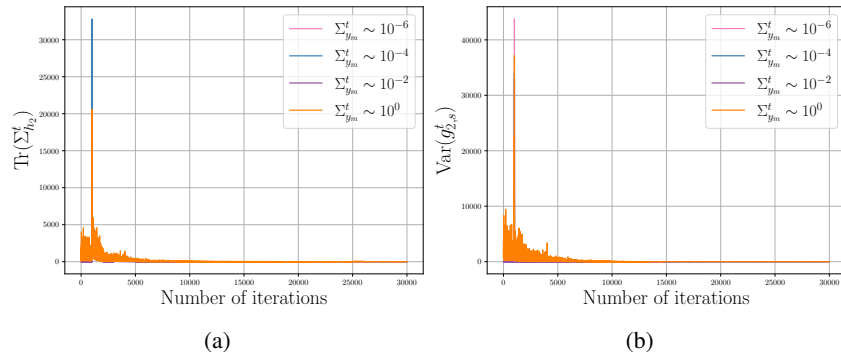


Figure 8: Uncertainty propagation in the communicated terms during FedGC learning for different regimes of $\Sigma_{y_m}^t$ (a) $\text{Var}(g_{m,s}^t)$ vs iterations, (b) $\Sigma_{h_m}^t$ vs iterations, in the synthetic dataset

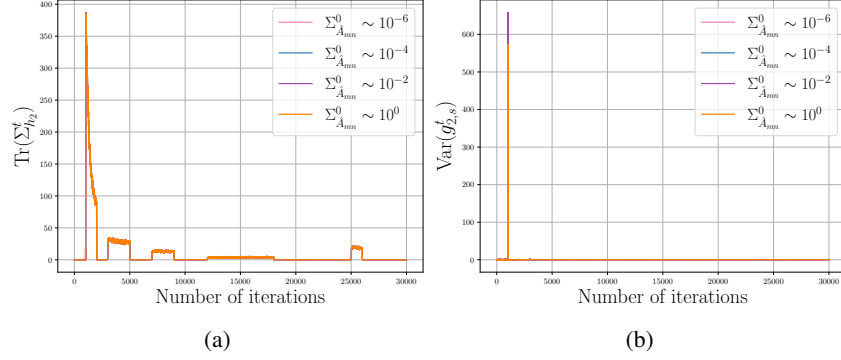


Figure 9: Uncertainty propagation in the communicated terms during FedGC learning for different regimes of $\Sigma_{\hat{A}_{mn}}^0$ (a) $\text{Var}(g_{m,s}^t)$ vs iterations, (b) $\Sigma_{h_m}^t$ vs iterations, in the synthetic dataset

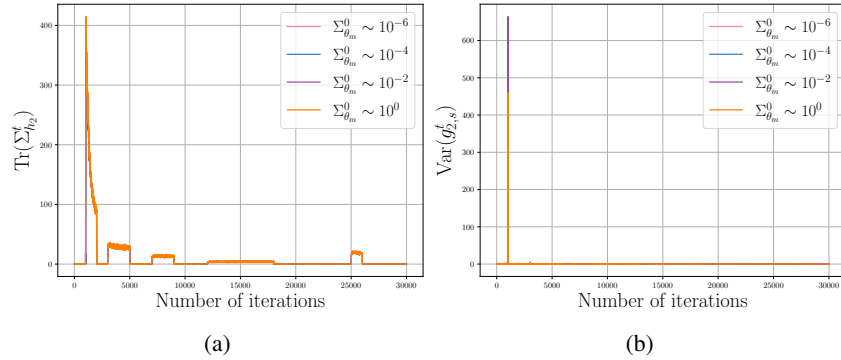


Figure 10: Uncertainty propagation in the communicated terms during FedGC learning for different regimes of $\Sigma_{\theta_m}^0$ (a) $\text{Var}(g_{m,s}^t)$ vs iterations, (b) $\Sigma_{h_m}^t$ vs iterations, in the synthetic dataset

Each sample is then projected into a two-dimensional local state space: $\mathbf{Z}^{(c)} = \tilde{\mathbf{Y}}^{(c)}\mathbf{B}^{(c)}$. To mildly couple the latent components, we apply the fixed transformation $M = \begin{bmatrix} 1 & 1 \\ 0 & 1 \end{bmatrix}$ such that, $\hat{\mathbf{Z}}^{(c)} = \mathbf{Z}^{(c)}M$. Finally, the transformed representation is standardized again using training statistics.

E.2 Nonlinear Experiments

Neural state-transition functions. Following Appendix J, we evaluate our framework on nonlinear dynamical systems by using Extended Kalman Filters (EKFs) at the clients augmented with LSTM networks. The server-side linear transition model is replaced by an LSTM, and local state transitions are likewise modeled with MLPs. Table 6 provides the experimental settings of these neural networks.

Generating states. To obtain low-dimensional latent states from the raw measurements, we apply singular value decomposition (SVD) to the stacked data matrix and retain the leading right singular vectors as the reduced state representation. Specifically, given the data matrix Y , we compute $Y = U\Sigma V^T$ and use the top- p columns of V to define the latent states. In this setting, the measurement function corresponds to the projection from the latent state back to the observation space induced by the retained singular vectors.

Results. Unlike linear FedGC, the server parameters in the nonlinear setting do not directly encode Granger causality. Instead, we analyze the Jacobian J of the server model, which acts as a time-dependent state-transition matrix and provides a notion of Granger causality. As in the linear case, we vary $\Sigma_{y_m}^t$ to study aleatoric uncertainty and perturb the hyperparameters of the nonlinear models discussed above to assess epistemic effects.

Fig. 11 shows an overall decreasing trend in the Jacobian uncertainty, with larger $\Sigma_{y_m}^t$ leading to slower convergence. Fig. 12 shows the evolution of uncertainty in the server Jacobian under

Table 6: Neural network architectures and hyperparameters used for nonlinear experiments on HAI dataset

Component	Model	Parameters
Server model	LSTM+FC (Fully Connected)	Hidden dim = 128 Num layers = 1 Activation = linear (FC) Optimizer = Adam, lr = 1×10^{-2}
Client augmentation model	LSTM + FC	Hidden dim = 32 Num layers = 1 Activation = linear (FC) Optimizer = Adam, lr = 1×10^{-4}
Client transition model	MLP (for EKF f_m)	Hidden layers = [64, 64] Activation = SiLU Optimizer = Adam, lr = 1×10^{-3}

different levels of noise in the server LSTM weights. Except at very high noise, all curves largely overlap, indicating minimal impact of epistemic initialization on Jacobian uncertainty. These results are consistent with the theoretical derivations in Section 6, particularly the nonlinear analogue of Theorem 6.4.

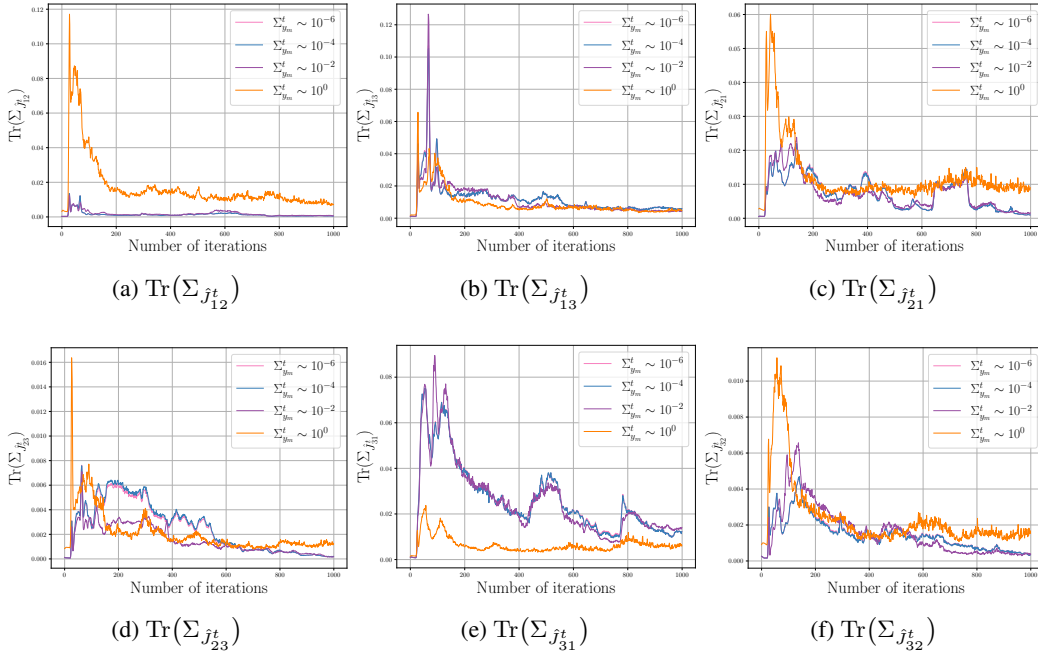


Figure 11: Nonlinear Exper. on HAI: Trace of the covariance for the off-diagonal blocks of the Jacobian matrix J for different $\Sigma_{y_m}^t$

F Experimental Compute Resources

All of the experiments were run locally on a 2022 MacBook Air with an Apple M2 chip, 16 GB unified memory, and 512 GB SSD storage. No cloud provider, computing cluster, or external GPU was used. The Apple M2 MacBook Air has an 8-core CPU with 4 performance cores and 4 efficiency cores, a 16-core Neural Engine, and 100 GB/s memory bandwidth; the 512 GB configuration is associated with the M2 configuration that can include the 10-core integrated GPU.

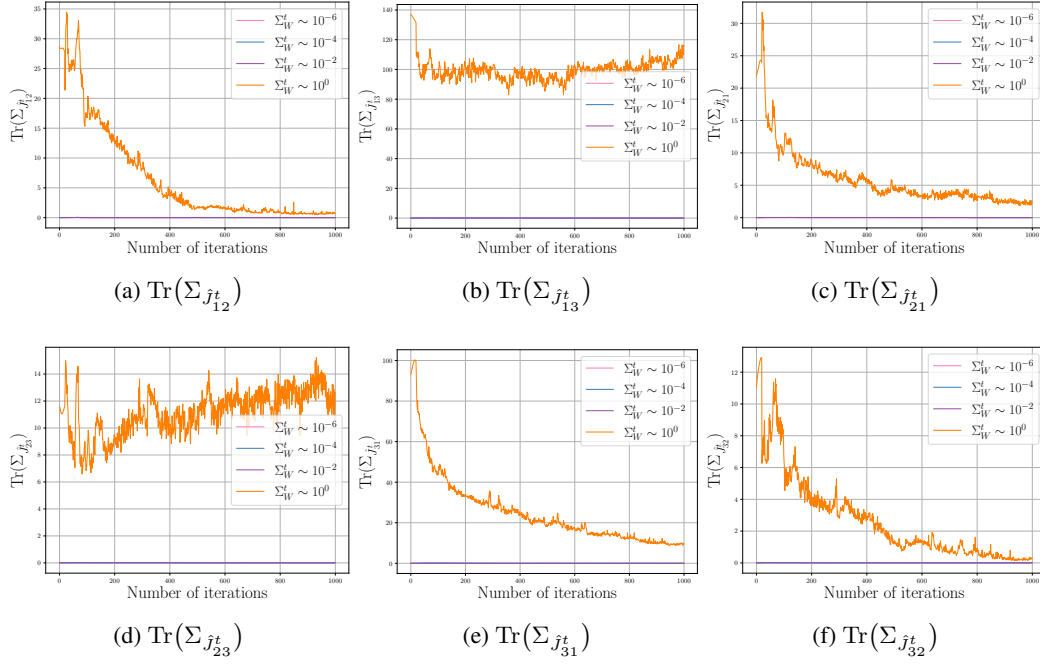


Figure 12: Nonlinear Exper. on HAI: Trace of the covariance for the off-diagonal blocks of the Jacobian matrix J for different Σ_W^t

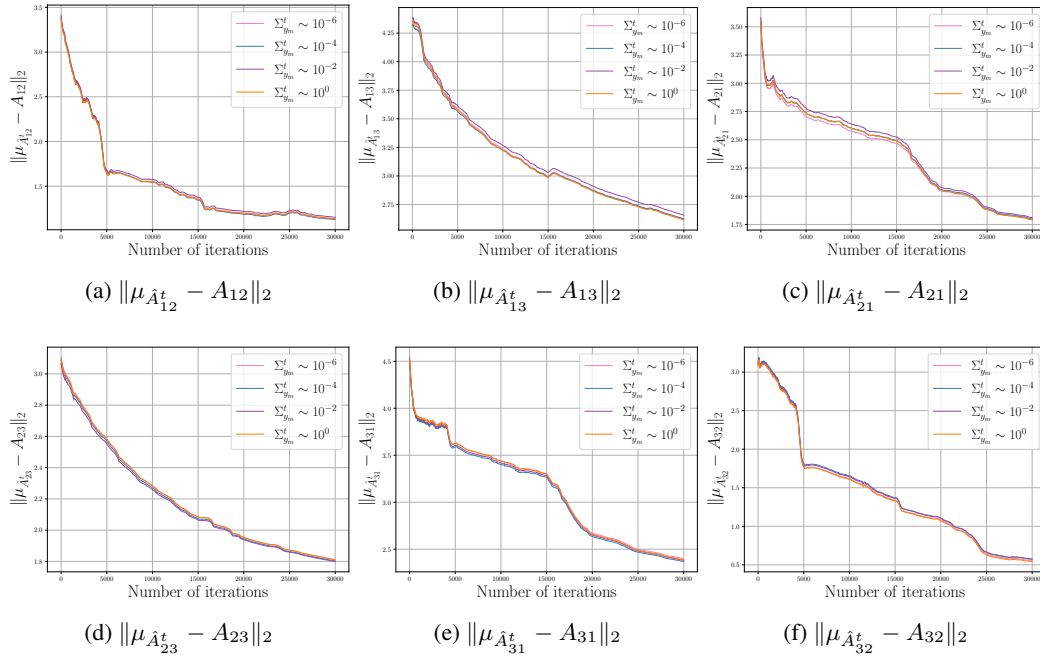


Figure 13: Average L_2 norm error of each off-diagonal block of the matrix A for different regimes of $\Sigma_{y_m}^t$ for HAI dataset

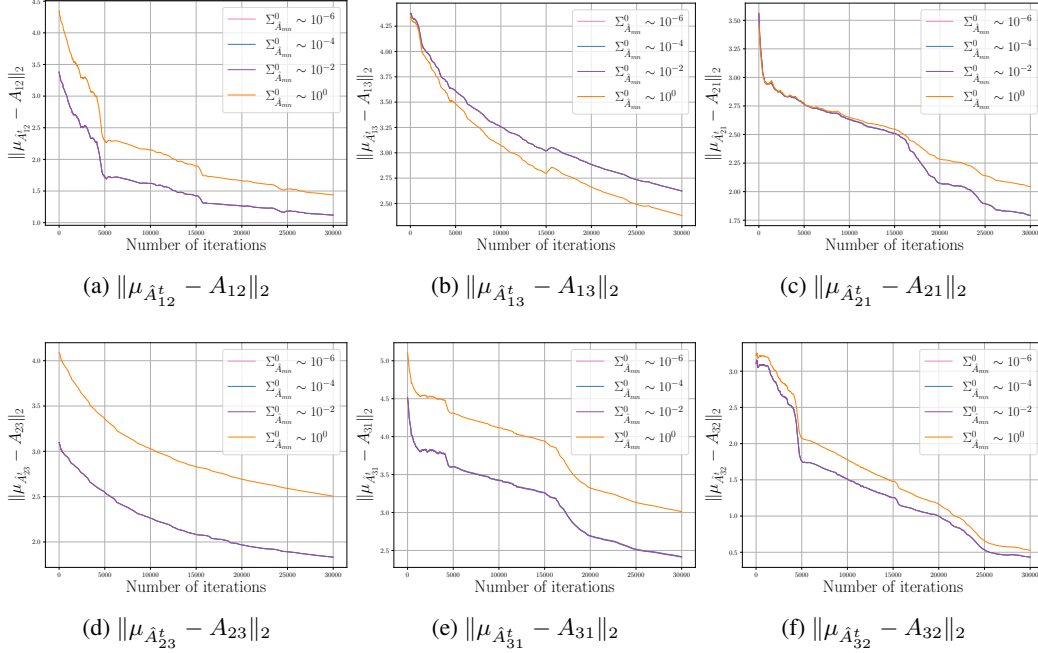


Figure 14: Average L_2 norm error of each off-diagonal block of the matrix A for different regimes of $\Sigma_{A_{mn}}^0$ for HAI dataset

G Supporting Theoretical Results for Assumptions in Section 4

G.1 Lemma G.1

Lemma G.1. *At any time t and, for each client m , define*

$$g_m = \nabla_{\theta_m} L_s = X_m (y_m^{t-1})^\top, \quad X_m := A_{mm}^\top \left(A_{mm} \Delta h_m - \sum_{r \neq m} \hat{A}_{mr} (\hat{h}_r^{t-1})_c \right).$$

Under Assumptions (A1)–(A4), we have for any $m \neq n$,

$$\text{Cov}(\text{vec}(g_m), \text{vec}(g_n)) = 0.$$

Proof. By Assumption (A2), the block-row server parameters for clients m and n are mutually independent, hence $X_m \perp X_n$. By Assumptions (A1), (A4), and (A5), the local data satisfy

$$\mu_{y_m} = \mathbb{E}[y_m^{t-1}], \quad \Sigma_{y_m} = \text{Cov}(y_m^{t-1}, y_m^{t-1}),$$

with $\text{Cov}(y_m^{t-1}, y_n^{t-1}) = 0$ for $m \neq n$. Since y_m^{t-1} is also independent of $\{A_{pq}^t\}$ by Assumption (A3), we may write

$$\text{vec}(g_m) = (I \otimes X_m) y_m^{t-1}.$$

Thus, for $m \neq n$,

$$\text{Cov}(\text{vec}(g_m), \text{vec}(g_n)) = \mathbb{E}[(I \otimes X_m) y_m^{t-1} (y_n^{t-1})^\top (I \otimes X_n)^\top] - \mathbb{E}[\text{vec}(g_m)] \mathbb{E}[\text{vec}(g_n)]^\top.$$

Independence allows factorization, and Assumption (A4)–(A5) implies $\mathbb{E}[y_m^{t-1} (y_n^{t-1})^\top] = \mu_{y_m} \mu_{y_n}^\top$, which cancels with the product of means. Hence

$$\text{Cov}(\text{vec}(g_m), \text{vec}(g_n)) = 0, \quad m \neq n.$$

□

G.2 Proposition G.2

Proposition G.2. Consider the client update rule

$$\theta_m^{t+1} = \theta_m^t - \eta_1 g_{m,a}^t - \eta_2 g_{m,s}^t,$$

where $g_{m,a}^t = \nabla_{\theta_m} L_m$ (local) and $g_{m,s}^t = \nabla_{\theta_m} L_s$ (global). Suppose Assumptions (A1)–(A5) hold. Then, for any two distinct clients $m \neq n$,

$$\lim_{t \rightarrow \infty} \text{Cov}(\theta_m^t, \theta_n^t) = 0.$$

Proof. Expanding the covariance for $m \neq n$ gives

$$\text{Cov}(\theta_m^{t+1}, \theta_n^{t+1}) = \text{Cov}(\theta_m^t, \theta_n^t) + \eta_2^2 \text{Cov}(g_{m,s}^t, g_{n,s}^t) + \text{vanishing local terms}$$

where the omitted terms involve cross-products between local and global gradients.

By Lemma G.1, $\text{Cov}(g_{m,s}^t, g_{n,s}^t) = 0$ for $m \neq n$. By (A2) and (A3), $\theta_m^t \perp\!\!\!\perp \theta_n^t$ at initialization. By (A4)–(A5), client data are uncorrelated across m, n , and all noise is additive. Hence all cross-terms vanish, and we obtain the recursion

$$\text{Cov}(\theta_m^{t+1}, \theta_n^{t+1}) = \text{Cov}(\theta_m^t, \theta_n^t).$$

Since the initial covariance is zero, induction gives $\text{Cov}(\theta_m^t, \theta_n^t) = 0$ for all t , and thus

$$\lim_{t \rightarrow \infty} \text{Cov}(\theta_m^t, \theta_n^t) = 0.$$

□

H Privacy Analysis

We formally prove that the cross-covariance terms between client quantities and server quantities can be made differentially private under the Gaussian mechanism.

FedGC Latent Privacy. In the original FedGC setup, each client m communicates a compressed latent state $\hat{h}_{c,m}^t$ and an augmented latent state $\hat{h}_{a,m}^t$, both of which are computed from private data y_m^t via local encoders (KF). As shown in Appendix F of FedGC, if the mapping $y_m^t \mapsto \hat{h}_{c,m}^t$ has bounded ℓ_2 -sensitivity Δ , then adding Gaussian noise:

$$\tilde{h}_{c,m}^t = \hat{h}_{c,m}^t + \mathcal{N}(0, \sigma^2 I), \quad \sigma \geq \frac{\Delta \cdot \sqrt{2 \log(1.25/\delta)}}{\varepsilon}$$

ensures (ε, δ) -differential privacy for each client's latent state. The same construction holds for $\hat{h}_{a,m}^t$ and is preserved in our framework.

DP for Cross-Covariances. Unlike FedGC, our method introduces server-side use of *cross-covariance* matrices between client representations, which may leak client-private correlations. The key objects are:

$$\Gamma_{mn}^t := \text{Cov}(\hat{h}_{c,m}^t, \hat{h}_{a,n}^t) = \mathbb{E}[\hat{h}_{c,m}^t (\hat{h}_{a,n}^t)^\top] - \bar{h}_{c,m}^t (\bar{h}_{a,n}^t)^\top$$

$$\Psi_{mn}^t := \text{Cov}(v_m^t, \hat{h}_{c,n}^t) = \mathbb{E}[v_m^t (\hat{h}_{c,n}^t)^\top] - \bar{v}_m^t (\bar{h}_{c,n}^t)^\top$$

where $v_m^t = \text{vec}(\theta_m^t)$ is the flattened client model parameter. We now show how to make these matrices differentially private via Gaussian noise.

Each client m transmits perturbed values of $\hat{h}_{c,m}^t, \hat{h}_{a,m}^t$

$$\tilde{h}_{c,m}^t = \hat{h}_{c,m}^t + \xi_c^t, \quad \tilde{h}_{a,n}^t = \hat{h}_{a,n}^t + \xi_a^t$$

with $\xi_c^t, \xi_a^t \sim \mathcal{N}(0, \sigma_h^2 I)$. Furthermore, since cross-covariance Ψ_{mn} requires v_m , we perturb it as:

$$\tilde{v}_m^t = v_m^t + \xi_v^t$$

with $\xi_v^t \sim \mathcal{N}(0, \sigma_v^2 I)$. The server then computes the cross-covariances:

$$\tilde{\Gamma}_{mn}^t := \text{Cov}(\tilde{h}_{c,m}^t, \tilde{h}_{a,n}^t), \quad \tilde{\Psi}_{mn}^t := \text{Cov}(\tilde{v}_m^t, \tilde{h}_{c,n}^t)$$

These estimators contain the desired cross-covariance along with stochastic masking from the perturbations.

Using classical state-space theory & Lipschitz assumptions, we have norm bounds: $\|\hat{h}_{c,m}^t\|_2 \leq B_c$, $\|\hat{h}_{a,n}^t\|_2 \leq B_a$, $\|v_m^t\|_2 \leq B_v$. Then, the ℓ_2 -sensitivities of Γ_{mn} , and Ψ_{mn} are:

$$\Delta_2(\Gamma_{mn}^t) \leq 2B_c B_a, \quad \Delta_2(\Psi_{mn}^t) \leq 2B_v B_c$$

To achieve (ϵ, δ) -DP via the Gaussian mechanism, it suffices to add i.i.d. noise to each element of the matrices:

$$\sigma_\Gamma \geq \frac{2B_c B_a \sqrt{2 \log(1.25/\delta)}}{\epsilon}, \quad \sigma_\Psi \geq \frac{2B_v B_c \sqrt{2 \log(1.25/\delta)}}{\epsilon}$$

This guarantees that the server-observed $\tilde{\Gamma}_{mn}^t$ and $\tilde{\Psi}_{mn}^t$ are differentially private with respect to any one client's data at time t .

Implications on Uncertainty Propagation. The injection of DP noise into Γ_{mn}^t and Ψ_{mn}^t affects the downstream uncertainty estimates in both client- and server-side propagation. Specifically, Γ_{mn}^t appears exclusively in the server-side recursion (Theorem 6.6), while both Γ_{mn}^t and Ψ_{mn}^t are used in the client-side update (Theorem 6.8). Making these matrices differentially private means that the propagated covariances become slightly biased or inflated due to the added noise. This leads to an overestimation of uncertainty, which preserves the structure of the recursion but may reduce the accuracy of Granger causality. Nonetheless, the estimates remain valid under perturbed inputs, and the user can control the privacy-utility trade-off via the (ϵ, δ) parameters.

I Complexity Analysis

Let each client m have state dimension p_m and data dimension d_m , with M clients in total. We first provide the computation and communication complexity per client.

(1) Computation. In a naive implementation, updating the full parameter covariance matrix $\Sigma_\theta^t \in \mathbb{R}^{p_m d_m \times p_m d_m}$ would incur $\mathcal{O}(p_m^2 d_m^2)$ computation per round due to matrix-matrix multiplications and Kronecker product evaluations. However, our implementation can avoid this cost by exploiting the structure of low-rank quantities such as $y^t y^{t\top}$ (which is rank-1), when $d_m \gg p_m$. As a result, matrix-vector products involving these terms can be computed without materializing the full $p_m d_m \times p_m d_m$ matrices. If we adopt a block-diagonal or factored representation of Σ_θ^t across layers or time steps, the per-client computational cost is further reduced to $\mathcal{O}(p_m d_m^2)$ per iteration.

(2) Communication. In terms of communication, our framework introduces no additional overhead compared to vanilla FedGC. Therefore, total communication cost per client remains $\mathcal{O}(p_m)$, matching that of FedGC. No additional communication is needed for tracking uncertainty.

All M clients. Across all M clients, the total additional computation scales as $\mathcal{O}\left(\sum_{m=1}^M p_m d_m^2\right)$ per round, while communication remains unchanged at $\mathcal{O}\left(\sum_{m=1}^M p_m\right)$. These properties make the method scalable to realistic federated settings.

J Extensions to the Framework

J.1 Non-Linear Models

Our current theory is derived under the assumption of linear time-invariant dynamics and Gaussian noise, consistent with the original FedGC model. Nonetheless, we emphasize that the structure of our uncertainty propagation is not inherently tied to linearity; it generalizes to any dynamical model with well-defined latent state compression and state transition.

We consider an extension to *nonlinear but stationary* dynamical systems. Nonlinear dynamics being highly model-specific, we first show that our theoretical structure carries over to two settings: (1)

Extended Kalman Filters (EKF) - non-linear extension of the linear KF based formulation, and (2) Gaussian Processes (GPs) - for kernelized settings. Both EKF, and GP-based frameworks support general nonlinear transition functions while admitting tractable recursive expressions analogous to Theorem 6.8.

(1) Extended Kalman Filter (EKF). EKF approximates nonlinear state transitions via first-order Taylor expansions. Consider the system:

$$h_c^t = f(h_c^{t-1}) + w^t, \quad y^t = g(h_c^t) + v^t, \quad w^t \sim \mathcal{N}(0, Q), \quad v^t \sim \mathcal{N}(0, R),$$

where $f: \mathbb{R}^p \rightarrow \mathbb{R}^p$, $g: \mathbb{R}^p \rightarrow \mathbb{R}^d$, with $d \gg p$, are smooth nonlinear functions. The prediction step linearizes f around the filtered mean:

$$\hat{h}_c^{t|t-1} = f(\hat{h}_c^{t-1}), \quad F^{t-1} := \left. \frac{\partial f}{\partial h} \right|_{h=\hat{h}_c^{t-1}}, \quad P^{t|t-1} = F^{t-1} P^{t-1} F^{t-1\top} + Q.$$

For the observation model, define $J_g := \left. \frac{\partial g}{\partial h} \right|_{h=\hat{h}_c^{t|t-1}}$. The update step proceeds via:

$$K^t = P^{t|t-1} J_g^\top (J_g P^{t|t-1} J_g^\top + R)^{-1}, \quad \hat{h}_c^t = \hat{h}_c^{t|t-1} + K^t (y^t - g(\hat{h}_c^{t|t-1})), \quad P^t = (I - K^t J_g) P^{t|t-1}.$$

We define the augmented representation used in FedGC:

$$\hat{h}_a^t = \hat{h}_c^t + \theta^t y^t, \quad \theta^t \in \mathbb{R}^{p \times d}, \quad v^t := \text{vec}(\theta^t).$$

Following our update rule, $v^{t+1} = v^t - \eta_1 \nabla_{v^t} \mathcal{L}_t^{\text{local}} - \eta_2 \nabla_{v^t} \mathcal{L}_t^{\text{server}}$, the parameter covariance update becomes:

$$\Sigma_\theta^{t+1} = H^t \Sigma_\theta^t H^{t\top} + G^t P^t G^{t\top} + H^t \Lambda^t G^{t\top} + G^t \Lambda^{t\top} H^t + P^t \Sigma_A^t P^{t\top},$$

where,

$$\begin{aligned} H^t &= I_{pd} - 2\eta_1 (y^t y^{t\top}) \otimes (J_g^\top J_g) - 2\eta_2 (y^t y^{t\top}) \otimes (A_{mm}^\top A_{mm}), \\ G^t &= 2\eta_1 (y^t \otimes J_g^\top), \\ P^t &= \text{Cov}(\hat{h}_c^t), \\ \Lambda^t &= \text{Cov}(v^t, \hat{h}_a^t). \end{aligned}$$

This recursion is structurally identical to Theorem 6.8, with C and P replaced by the Jacobian J_g and EKF posterior P^t , respectively.

(2) Gaussian Process (GP). Consider a GP-based transition model, where $f \sim \mathcal{GP}(0, k(\cdot, \cdot))$ governs the latent dynamics:

$$h_c^t = f(h_c^{t-1}) + w^t.$$

Conditioning on past data $\{h_c^i, h_c^{i-1}\}_{i=1}^n$, the GP posterior yields:

$$h_c^t \sim \mathcal{N}(\mu_t^f, \Sigma_t^f + Q), \quad \mu_t^f = k^\top(h_c^{t-1}) K^{-1} \mathbf{h}, \quad \Sigma_t^f = k(h_c^{t-1}, h_c^{t-1}) - k^\top(h_c^{t-1}) K^{-1} k(h_c^{t-1}),$$

where K is the kernel matrix over $\{h_c^{i-1}\}$. We again define:

$$\hat{h}_a^t = \mu_t^f + \theta^t y^t.$$

The parameter covariance propagates as:

$$\Sigma_\theta^{t+1} = H^t \Sigma_\theta^t H^{t\top} + G^t \Sigma_t^f G^{t\top} + H^t \Lambda^t G^{t\top} + G^t \Lambda^{t\top} H^t + P^t \Sigma_A^t P^{t\top},$$

with $J_g := \partial g / \partial h|_{h=\mu_t^f}$ and other terms as above. This recursion mirrors the EKF case, with GP posterior variance Σ_t^f replacing P^t , and confirms that Theorem 6.8 applies structurally to kernelized approximations.

J.2 Relaxing Stationary Assumptions

Our main theoretical results are derived under the classical assumption that each client observes weakly stationary data with time-invariant first- and second-order moments. This assumption enables closed-form uncertainty propagation through the FedGC recursions. Here we clarify how the framework behaves when stationarity is mildly violated and how it can be adapted to non-stationary settings.

Exponentially weighted moments. The key observation is that all uncertainty recursions remain valid when the empirical moments are replaced by *exponentially weighted* (EWMA) moments,

$$\mu_t = (1 - \lambda)\mu_{t-1} + \lambda x_t, \quad \Sigma_t = (1 - \lambda)\Sigma_{t-1} + \lambda x_t x_t^\top,$$

for a forgetting factor $0 < \lambda < 1$. Suppose the underlying data possess slowly drifting moments (μ_t^*, Σ_t^*) with bounded temporal variation $\|\mu_t^* - \mu_{t-1}^*\| \leq \delta$ and $\|\Sigma_t^* - \Sigma_{t-1}^*\| \leq \delta$. Standard results for stochastic approximation imply

$$\|\mu_t - \mu_t^*\| = O(\delta/\lambda), \quad \|\Sigma_t - \Sigma_t^*\| = O(\delta/\lambda).$$

Thus, EWMA moments track the true time-varying moments whenever the drift is slower than the forgetting rate. Replacing stationary moments by EWMA moments preserves the algebraic form of our uncertainty recursions; the same propagation equations apply with (μ_t, Σ_t) in place of fixed moments.

Beyond EWMA, other forms of non-stationarity can be incorporated by modifying the moment-estimation step. Examples include sliding-window estimators, seasonally adjusted or periodic-window estimators, trend-filtered or total-variation-regularized moment updates, and online convex-combination estimators for abrupt regime changes. Neural-network-based models can also accommodate complex non-stationarity, but doing so would require deriving a new set of uncertainty-propagation equations beyond the linear FedGC framework. A systematic treatment of these extensions is an important direction for future work.

K Proofs

K.1 Proposition 6.1

• **Proposition (Client Model-Client Data Dependence)** Assume $\text{Var}(y_m^{t-1}) > 0$. Then under the federated Granger-causality updates, $\Omega_m^t := \text{Cov}(v_m^t, y_m^t) \neq 0$.

Proof. From the gradient-descent update we have,

$$\begin{aligned} \theta_m^t &= \theta_m^{t-1} + 2\eta_1 (C_{mm} A_{mm})^\top (y_m^t - C_{mm} A_{mm} [\hat{h}_{m,c}^{t-1} + \theta_m^{t-1} y_m^{t-1}]) y_m^{t-1\top} \\ &\quad - 2\eta_2 A_{mm}^\top \left(A_{mm} [\hat{h}_{m,a}^{t-1} - \hat{h}_{m,c}^{t-1}] - \sum_{n \neq m} \hat{A}_{mn}^{t-1} \hat{h}_{n,c}^{t-1} \right) y_m^{t-1\top}. \end{aligned}$$

Rearrange to isolate dependence on y_m^{t-1} :

$$\theta_m^t = M + B y_m^{t-1\top},$$

where

$$\begin{aligned} M &= \theta_m^{t-1} + 2\eta_1 (C_{mm} A_{mm})^\top (y_m^t - C_{mm} A_{mm} \hat{h}_{m,c}^{t-1}) y_m^{t-1\top} - 2\eta_2 A_{mm}^\top \left(A_{mm} [\hat{h}_{m,a}^{t-1} - \hat{h}_{m,c}^{t-1}] \right) y_m^{t-1\top}, \\ B &= -2\eta_1 (C_{mm} A_{mm})^\top C_{mm} A_{mm} \theta_m^{t-1} - 2\eta_2 A_{mm}^\top \sum_{n \neq m} \hat{A}_{mn}^{t-1} \hat{h}_{n,c}^{t-1}. \end{aligned}$$

Thus $\theta_m^t = M + B y_m^{t-1\top}$ is an affine function of y_m^{t-1} .

Furthermore, the LTI measurement model gives

$$y_m^t = C_{mm} A_{mm} \hat{h}_{m,a}^{t-1} + \text{Var} \epsilon_m^t = C_{mm} A_{mm} (\hat{h}_{m,c}^{t-1} + \theta_m^{t-1} y_m^{t-1}) + \text{Var} \epsilon_m^t.$$

Rearranging we obtain,

$$y_m^t = N + D y_m^{t-1} + \text{Var} \epsilon_m^t,$$

where,

$$N = C_{mm} A_{mm} \hat{h}_{m,c}^{t-1}, \quad D = C_{mm} A_{mm} \theta_m^{t-1}.$$

Thus y_m^t is also an affine function of y_m^{t-1} .

Let $u = y_m^{t-1}$. Then

$$\theta_m^t = M + B u^\top, \quad y_m^t = N + D u + \text{Var} \epsilon_m^t.$$

Since $\text{Var} \epsilon_m^t$ is zero-mean and independent of u , we have

$$\text{Cov}(\theta_m^t, y_m^t) = \text{Cov}(M + B u^\top, N + D u) = B \text{Cov}(u^\top, u) D^\top = B \text{Var}(u) D^\top.$$

By assumption $\text{Var}(u) = \text{Var}(y_m^{t-1}) > 0$, and B, D are nonzero (since the update and measurement matrices are full-rank). Therefore $\text{Cov}(\theta_m^t, y_m^t) = B \text{Var}(y_m^{t-1}) D^\top \neq 0$.

Hence $\Omega_m^t \neq 0$, as claimed. \square

K.2 Proposition 6.2

• **Proposition (Client Model-Client State Dependence)** *Let $\Lambda_m^t = \text{Cov}(v_m^t, \hat{h}_{m,a}^t)$. Then we have the following recursion within the client, $\Lambda_m^t = \Sigma_{\theta_m}^t (I_{d_m} \otimes \mu_{y_m}^t) + \Omega_m^t (\mu_{v_m}^t \otimes I_{d_m})$,*

Proof. We prove the recursion for $\Lambda_m^t = \text{Cov}(v_m^t, \hat{h}_{m,a}^t)$ using the paper's definitions:

From Table 1 and Eq. (4), we have the following definitions,

$$\begin{aligned} \Sigma_{\theta_m}^t &:= \text{Var}(v_m^t) = \mathbb{E}[v_m^t v_m^{t\top}] - \mu_{\theta_m}^t \mu_{\theta_m}^{t\top} \\ \Omega_m^t &:= \text{Cov}(v_m^t, y_m^t) = \mathbb{E}[v_m^t y_m^{t\top}] - \mu_{\theta_m}^t \mu_{y_m}^{t\top} \\ \hat{h}_{m,a}^t &:= \hat{h}_{m,c}^t + \theta_m^t y_m^t = \hat{h}_{m,c}^t + (y_m^{t\top} \otimes I_{p_m}) v_m^t \end{aligned}$$

Expanding Λ_m^t from first principles, and using the definition of $\hat{h}_{m,a}^t$ we have,

$$\begin{aligned} \Lambda_m^t &= \mathbb{E}[v_m^t \hat{h}_{m,a}^{t\top}] - \mu_{\theta_m}^t \mu_{h_{m,a}}^{t\top} \\ &= \mathbb{E} \left[v_m^t \left(\hat{h}_{m,c}^{t\top} + v_m^{t\top} (y_m^t \otimes I_{p_m}) \right) \right] - \mu_{\theta_m}^t \left(\hat{h}_{m,c}^{t\top} + \mu_{\theta_m}^{t\top} (\mu_{y_m}^t \otimes I_{p_m}) \right) \\ &= \mathbb{E}[v_m^t v_m^{t\top} (y_m^t \otimes I_{p_m})] - \mu_{\theta_m}^t \mu_{\theta_m}^{t\top} (\mu_{y_m}^t \otimes I_{p_m}) \end{aligned}$$

Analyzing the key expectation terms and substituting the definitions of $\Sigma_{\theta_m}^t$, and Ω_m^t we have,

$$\begin{aligned} \mathbb{E}[v_m^t v_m^{t\top} (y_m^t \otimes I_{p_m})] &= \mathbb{E} \left[(\Sigma_{\theta_m}^t + \mu_{\theta_m}^t \mu_{\theta_m}^{t\top}) (y_m^t \otimes I_{p_m}) \right] \quad (\text{since } \mathbb{E}[v_m^t v_m^{t\top}] = \Sigma_{\theta_m}^t + \mu_{\theta_m}^t \mu_{\theta_m}^{t\top}) \\ &= \Sigma_{\theta_m}^t (\mu_{y_m}^t \otimes I_{p_m}) + \mu_{\theta_m}^t \mu_{\theta_m}^{t\top} (\mu_{y_m}^t \otimes I_{p_m}) \\ &\quad + \mathbb{E}[(v_m^t - \mu_{\theta_m}^t)(v_m^t - \mu_{\theta_m}^t)^\top (y_m^t - \mu_{y_m}^t \otimes I_{p_m})] \\ &= \Sigma_{\theta_m}^t (\mu_{y_m}^t \otimes I_{p_m}) + \mu_{\theta_m}^t \mu_{\theta_m}^{t\top} (\mu_{y_m}^t \otimes I_{p_m}) \\ &\quad + \mu_{\theta_m}^t \mathbb{E}[(v_m^t - \mu_{\theta_m}^t)(y_m^t - \mu_{y_m}^t)^\top] \otimes I_{p_m} \\ &= \Sigma_{\theta_m}^t (\mu_{y_m}^t \otimes I_{p_m}) + \mu_{\theta_m}^t \mu_{\theta_m}^{t\top} (\mu_{y_m}^t \otimes I_{p_m}) + \mu_{\theta_m}^t \Omega_m^{t\top} \otimes I_{p_m} \end{aligned}$$

Substituting the expression for $\mathbb{E}[v_m^t v_m^{t\top} (y_m^t \otimes I_{p_m})]$ (obtained above), back into Λ_m^t we have,

$$\begin{aligned} \Lambda_m^t &= (\Sigma_{\theta_m}^t (\mu_{y_m}^t \otimes I_{p_m}) + \mu_{\theta_m}^t \mu_{\theta_m}^{t\top} (\mu_{y_m}^t \otimes I_{p_m}) + \mu_{\theta_m}^t \Omega_m^{t\top} \otimes I_{p_m}) \\ &\quad - \mu_{\theta_m}^t \mu_{\theta_m}^{t\top} (\mu_{y_m}^t \otimes I_{p_m}) \\ &= \Sigma_{\theta_m}^t (\mu_{y_m}^t \otimes I_{p_m}) + \mu_{\theta_m}^t \Omega_m^{t\top} \otimes I_{p_m} \end{aligned}$$

Recognizing that $\Omega_m^{t\top} \otimes I_{p_m} = (\Omega_m^t \otimes I_{p_m})^\top$, and simplifying the second term we obtain,

$$\mu_{\theta_m}^t \Omega_m^{t\top} \otimes I_{p_m} = (\Omega_m^t \otimes I_{p_m}) \mu_{\theta_m}^t = \Omega_m^t (\mu_{\theta_m}^t \otimes I_{d_m})$$

Substituting this into the expression for Λ_m^t we have,

$$\Lambda_m^t = \Sigma_{\theta_m}^t (I_{d_m} \otimes \mu_{y_m}^t) + \Omega_m^t (\mu_{\theta_m}^t \otimes I_{d_m})$$

\square

K.3 Lemma 6.3

Assumption (A6): The client's augmented hidden state changes only by a small amount between two consecutive time-steps $\Delta h_m^t := \hat{h}_{m,a}^{t+1} - \hat{h}_{m,a}^t$ satisfying $\|\Delta h_m^t\|_2 \leq \varepsilon$ with ε is small.

• **Lemma (Client State-Sever Model Dependence)** The cross-covariance term $\Gamma_{mn}^t := \text{Cov}(a_{mn}^t, \hat{h}_{m,a}^t)$ follows the recursive equation: $\Gamma_{mn}^{t+1} = D_n^t \Gamma_{mn}^t + 2\gamma B_{mn}^t \Sigma_{h_m}^t$ where, $D_n^t = (I - 2\gamma \hat{h}_{n,c}^t \hat{h}_{n,c}^{t\top}) \otimes I$, $B_{mn}^t = \hat{h}_{n,c}^t \otimes A_{mm}$, and $\Sigma_{h_m}^t = \text{Var}(\hat{h}_{m,a}^t)$.

Proof. Gradient descent on the quadratic loss L_s with step size γ gives,

$$a_{mn}^{t+1} = D_n^t a_{mn}^t + 2\gamma B_{mn}^t \hat{h}_{m,a}^t,$$

where $D_n^t = (I - 2\gamma \hat{h}_{n,c}^t \hat{h}_{n,c}^{t\top}) \otimes I$ and $B_{mn}^t = \hat{h}_{n,c}^t \otimes A_{mm}$.

Taking the column covariance with $\hat{h}_{m,a}^t$ yields the shifted covariance term

$$\tilde{\Gamma}_{mn}^{t+1} := \text{Cov}(a_{mn}^{t+1}, \hat{h}_{m,a}^t) = D_n^t \Gamma_{mn}^t + 2\gamma B_{mn}^t \Sigma_{h_m}^t.$$

By Assumption (A6),

$$\hat{h}_{m,a}^{t+1} = \hat{h}_{m,a}^t + \Delta h_m^t, \quad \|\Delta h_m^t\|_2 \leq \varepsilon.$$

Defining, $\Gamma_{mn}^{t+1} := \text{Cov}(a_{mn}^{t+1}, \hat{h}_{m,a}^{t+1})$ and expanding, we get,

$$\Gamma_{mn}^{t+1} = \text{Cov}(a_{mn}^{t+1}, \hat{h}_{m,a}^t + \Delta h_m^t)$$

Let us define $E_{mn}^t := \text{Cov}(a_{mn}^{t+1}, \hat{h}_{m,a}^t + \Delta h_m^t)$. Thne the matrix Cauchy–Schwarz inequality gives,

$$\|E_{mn}^t\|_2 \leq \sqrt{\text{tr}(\Sigma_{A_{mn}}^{t+1})} \varepsilon = O(\varepsilon).$$

Using the above expression we obtain,

$$\Gamma_{mn}^{t+1} = D_n^t \Gamma_{mn}^t + 2\gamma B_{mn}^t \Sigma_{h_m}^t + O(\varepsilon),$$

If ε is small (Assumption (A6)), we get,

$$\Gamma_{mn}^{t+1} = D_n^t \Gamma_{mn}^t + 2\gamma B_{mn}^t \Sigma_{h_m}^t$$

□

K.4 Lemma 6.4

• **Lemma (Client Model-Server Model Dependence)** The term $\Psi_{mn}^t := \text{Cov}(a_{mn}^t, v_m^t)$ evolves as, $\Psi_{mn}^{t+1} = D_n^t \Psi_{mn}^t H_m^{t\top} + D_n^t \Gamma_{mn}^t G_m^{t\top} - D_n^t \Sigma_{A_{mn}}^t P_m^{t\top} + 2\gamma B_{mn}^t \Lambda_m^t H_m^{t\top} + 2\gamma B_{mn}^t \Sigma_{h_m}^t G_m^{t\top} - 2\gamma B_{mn}^t \Gamma_{mn}^{t\top} P_m^{t\top}$, with the following gain matrices, $B_{mn}^t = \hat{h}_{n,c}^t \otimes A_{mm}$,

$$D_n^t = (I - 2\gamma \hat{h}_{n,c}^t \hat{h}_{n,c}^{t\top}) \otimes I, G_m^t = 2\eta_1 (y_m^t \otimes (C_{mm} A_{mm})^\top), P_m^t = -2\eta_2 (y_m^t \otimes A_{mm}^\top)$$

and $H_m^t = I_{p_m d_m} - 2\eta_1 (y_m^t y_m^{t\top}) \otimes ((C_{mm} A_{mm})^\top C_{mm} A_{mm}) - 2\eta_2 (y_m^t y_m^{t\top}) \otimes (A_{mm}^\top A_{mm})$

Proof. From the loss L_s one gradient–descent step with stepsize γ gives,

$$a_{mn}^{t+1} = D_n^t a_{mn}^t + 2\gamma B_{mn}^t \hat{h}_{m,a}^t.$$

The update $\theta_m^{t+1} = \theta_m^t - \eta_1 \nabla_{\theta_m} (L_m)_a - \eta_2 \nabla_{\theta_m} L_s$ is linear in $(\theta_m^t, \hat{h}_{m,a}^t, a_{mn}^t)$; in vectorized form,

$$v_m^{t+1} = H_m^t v_m^t + G_m^t \hat{h}_{m,a}^t - P_m^t a_{mn}^t.$$

Compute $\Psi_{mn}^{t+1} = \text{Cov}(a_{mn}^{t+1}, v_m^{t+1})$ using the above two equations,

$$\begin{aligned} \Psi_{mn}^{t+1} &= \text{Cov}(D_n^t a_{mn}^t + 2\gamma B_{mn}^t \hat{h}_{m,a}^t, H_m^t v_m^t + G_m^t \hat{h}_{m,a}^t - P_m^t a_{mn}^t) \\ &= D_n^t \text{Cov}(a_{mn}^t, v_m^t) H_m^{t\top} + D_n^t \text{Cov}(a_{mn}^t, \hat{h}_{m,a}^t) G_m^{t\top} - D_n^t \text{Cov}(a_{mn}^t, a_{mn}^t) P_m^{t\top} \\ &\quad + 2\gamma B_{mn}^t \text{Cov}(\hat{h}_{m,a}^t, v_m^t) H_m^{t\top} + 2\gamma B_{mn}^t \text{Cov}(\hat{h}_{m,a}^t, \hat{h}_{m,a}^t) G_m^{t\top} - 2\gamma B_{mn}^t \text{Cov}(\hat{h}_{m,a}^t, a_{mn}^t) P_m^{t\top} \\ &= D_n^t \Psi_{mn}^t H_m^{t\top} + D_n^t \Gamma_{mn}^t G_m^{t\top} - D_n^t \Sigma_{A_{mn}}^t P_m^{t\top} + 2\gamma B_{mn}^t \Lambda_m^t H_m^{t\top} + 2\gamma B_{mn}^t \Sigma_{h_m}^t G_m^{t\top} - 2\gamma B_{mn}^t \Gamma_{mn}^{t\top} P_m^{t\top}. \end{aligned}$$

Grouping the six contributions yields the given recursion of Ψ_{mn}^{t+1} . □

K.5 Lemma 6.5

• **Lemma (Uncertainty in Client to Server Communication)** Let $\kappa_m = \text{tr}(\Sigma_{y_m}^t) + \|\mu_{y_m}^t\|^2$. Then the variance in the $\hat{h}_{m,a}^t$ is given by, $\Sigma_{h_m}^t = \kappa_m \Sigma_{\theta_m}^t + \Omega_m^t (\mu_{y_m}^t \otimes I_{p_m})^\top + (\mu_{y_m}^t \otimes I_{p_m}) \Omega_m^{t\top}$.

Proof. From the definition of augmented client states we have, $q_m^t := \hat{h}_{m,a}^t - \hat{h}_{m,c}^t = \theta_m^t y_m^t$, which in vectorized form is $q_m^t := Y_m^t v_m^t$, with $Y_m^t := (y_m^{t\top} \otimes I_{p_m})$. Therefore, by definition we have,

$$\text{Var}(q_m^t) = \mathbb{E}[Y_m^t v_m^t v_m^{t\top} Y_m^{t\top}] - \mathbb{E}[Y_m^t v_m^t] \mathbb{E}[Y_m^t v_m^t]^\top.$$

Computing the second moment we have,

$$\begin{aligned} \mathbb{E}[Y_m^t v_m^t v_m^{t\top} Y_m^{t\top}] &= \mathbb{E}[(y_m^t \otimes I_{p_m}) v_m^t v_m^{t\top} (y_m^{t\top} \otimes I_{p_m})] \\ &= \mathbb{E}[(y_m^t y_m^{t\top}) \otimes (v_m^t v_m^{t\top})] \\ &= \mathbb{E}[y_m^t y_m^{t\top}] \otimes \mathbb{E}[v_m^t v_m^{t\top}] + \text{Cov}(y_m^t \otimes v_m^t) \\ &= (\Sigma_{y_m}^t + \mu_{y_m}^t \mu_{y_m}^{t\top}) \otimes (\Sigma_{\theta_m}^t + \mu_{\theta_m}^t \mu_{\theta_m}^{t\top}) \\ &\quad + \Omega_m^t \otimes (\mu_{y_m}^t \otimes I_{p_m})^\top + (\mu_{y_m}^t \otimes I_{p_m}) \otimes \Omega_m^{t\top}. \end{aligned}$$

The first moment is given by,

$$\mathbb{E}[Y_m^t v_m^t] = (\mu_{y_m}^t \otimes I_{p_m}) \mu_{\theta_m}^t + \Omega_m^t$$

Computing the outer product of the first moments we have,

$$\begin{aligned} \mathbb{E}[Y_m^t v_m^t] \mathbb{E}[Y_m^t v_m^t]^\top &= (\mu_{y_m}^t \mu_{y_m}^{t\top}) \otimes (\mu_{\theta_m}^t \mu_{\theta_m}^{t\top}) \\ &\quad + \Omega_m^t (\mu_{y_m}^t \otimes I_{p_m})^\top + (\mu_{y_m}^t \otimes I_{p_m}) \Omega_m^{t\top}. \end{aligned}$$

Subtracting outer product of first moment from second moment we obtain,

$$\begin{aligned} \text{Var}(q_m^t) &= [(\Sigma_{y_m}^t + \mu_{y_m}^t \mu_{y_m}^{t\top}) \otimes \Sigma_{\theta_m}^t] + [(\Sigma_{y_m}^t + \mu_{y_m}^t \mu_{y_m}^{t\top}) \otimes \mu_{\theta_m}^t \mu_{\theta_m}^{t\top}] \\ &\quad - (\mu_{y_m}^t \mu_{y_m}^{t\top}) \otimes (\mu_{\theta_m}^t \mu_{\theta_m}^{t\top}) \\ &\quad + \Omega_m^t (\mu_{y_m}^t \otimes I_{p_m})^\top + (\mu_{y_m}^t \otimes I_{p_m}) \Omega_m^{t\top}. \end{aligned}$$

The term $(\Sigma_{y_m}^t + \mu_{y_m}^t \mu_{y_m}^{t\top}) \otimes \mu_{\theta_m}^t \mu_{\theta_m}^{t\top} - \mu_{y_m}^t \mu_{y_m}^{t\top} \otimes \mu_{\theta_m}^t \mu_{\theta_m}^{t\top}$ simplifies to $\Sigma_{y_m}^t \otimes \mu_{\theta_m}^t \mu_{\theta_m}^{t\top}$. By design, $\Sigma_{y_m}^t \otimes \mu_{\theta_m}^t \mu_{\theta_m}^{t\top}$ is absorbed into $\kappa_m \Sigma_{\theta_m}^t$ via trace normalization, leaving,

$$\text{Var}(q_m^t) = \kappa_m \Sigma_{\theta_m}^t + \Omega_m^t (\mu_{y_m}^t \otimes I_{p_m})^\top + (\mu_{y_m}^t \otimes I_{p_m}) \Omega_m^{t\top}.$$

Using the definition of q_m^t we have,

$$\text{Var}(\hat{h}_{m,a}^t - \hat{h}_{m,c}^t) = \kappa_m \Sigma_{\theta_m}^t + \Omega_m^t (\mu_{y_m}^t \otimes I_{p_m})^\top + (\mu_{y_m}^t \otimes I_{p_m}) \Omega_m^{t\top}.$$

Since $\hat{h}_{m,c}^t$ is deterministic, we have,

$$\Sigma_{h_m}^t := \text{Var}(\hat{h}_{m,a}^t) = \kappa_m \Sigma_{\theta_m}^t + \Omega_m^t (\mu_{y_m}^t \otimes I_{p_m})^\top + (\mu_{y_m}^t \otimes I_{p_m}) \Omega_m^{t\top}.$$

□

K.6 Lemma 6.6

• **Lemma (Uncertainty in Server to Client Communication)** With notation as above, the uncertainty in the gradient communicated by the server is given by, $\text{Var}(g_{m,s}^{t+1}) = A_{mm}^\top U^t A_{mm}$, where $U^t = A_{mm} \Sigma_{h_m}^t A_{mm}^\top + \sum_{n \neq m} (h_{n,c}^t h_{n,c}^{t\top}) \Sigma_{A_{mn}}^t - 2 \sum_{n \neq m} A_{mm} \Gamma_{mn}^t h_{n,c}^{t\top}$.

Proof. Let $r^t := A_{mm}(\hat{h}_{m,a}^t - \hat{h}_{m,c}^t) - \sum_{n \neq m} \hat{A}_{mn}^t \hat{h}_{n,c}^t$. We know that, $g_{m,s}^{t+1} = A_{mm}^\top r^t$. Then

$$\text{Var}(g_{m,s}^{t+1}) = A_{mm}^\top \text{Var}(r^t) A_{mm}.$$

We compute

$$\text{Var}(r^t) := \text{Var}(A_{mm} \hat{h}_{m,a}^t) + \sum_{n \neq m} \text{Var}(\hat{A}_{mn}^t \hat{h}_{n,c}^t) - 2 \sum_{n \neq m} \text{Cov}(A_{mm} \hat{h}_{m,a}^t, \hat{A}_{mn}^t \hat{h}_{n,c}^t),$$

Since $\hat{h}_{m,c}^t$ is deterministic. We have,

$$\text{Var}(A_{mm} \hat{h}_{m,a}^t) = A_{mm} \Sigma_{h_m}^t A_{mm}^\top,$$

$$\text{Var}(\hat{A}_{mn}^t \hat{h}_{n,c}^t) = (h_{n,c}^t h_{n,c}^{t\top}) \Sigma_{A_{mn}}^t; \text{Cov}(A_{mm} \hat{h}_{m,a}^t, \hat{A}_{mn}^t \hat{h}_{n,c}^t) = A_{mm} \Gamma_{mn}^t h_{n,c}^{t\top}.$$

Putting these into $\text{Var}(r^t)$ gives exactly

$$U^t = A_{mm} \Sigma_{h_m}^t A_{mm}^\top + \sum_{n \neq m} (h_{n,c}^t h_{n,c}^{t\top}) \Sigma_{A_{mn}}^t - 2 \sum_{n \neq m} A_{mm} \Gamma_{mn}^t h_{n,c}^{t\top}.$$

Hence $\text{Var}(g_{m,s}^{t+1}) = A_{mm}^\top U^t A_{mm}$, as claimed. \square

K.7 Theorem 6.7

• **Theorem (Uncertainty Propagation within the Server)** *The server model parameter a_{mn}^t 's covariance $\Sigma_{A_{mn}}^t$ evolves as, $\Sigma_{A_{mn}}^{t+1} = D_n^t \Sigma_{A_{mn}}^t D_n^{t\top} + 4\gamma^2 (\hat{h}_{n,c}^t \otimes A_{mm}) \Sigma_{h_m}^t (\hat{h}_{n,c}^t \otimes A_{mm})^\top + 2\gamma (D_n^t \Gamma_{mn}^t B_{mn}^{t\top} + B_{mn}^t \Gamma_{mn}^{t\top} D_n^{t\top})$ with $D_n^t = (I - 2\gamma \hat{h}_{n,c}^t \hat{h}_{n,c}^{t\top}) \otimes I$, and $B_{mn}^t = \hat{h}_{n,c}^t \otimes A_{mm}$*

Proof. At round t , the server gradient update as follows:

$$\hat{A}_{mn}^{t+1} = \hat{A}_{mn}^t (I - 2\gamma \hat{h}_{n,c}^t \hat{h}_{n,c}^{t\top}) + 2\gamma A_{mm} [\hat{h}_{m,a}^t - \hat{h}_{m,c}^t] \hat{h}_{n,c}^{t\top} - 2\gamma \sum_{p \neq m, n} \hat{A}_{mp}^t \hat{h}_{p,c}^t \hat{h}_{n,c}^{t\top}.$$

Under Assumption **(A1)** (off-diagonal blocks independent), the last summation term contributes no covariance with \hat{A}_{mn}^t and can be omitted when computing $\text{Var}(\hat{A}_{mn}^{t+1})$.

Apply $\text{Vec}(\cdot)$ and use the property that: $\text{Vec}(XB) = (B^\top \otimes I) \text{Vec}(X)$ and $\text{Vec}(AX) = (I \otimes A) \text{Vec}(X)$ for any three matrices A, B, X .

We obtain the following after vectorization,

$$\text{Vec}(\hat{A}_{mn}^{t+1}) = \left((I - 2\gamma \hat{h}_{n,c}^t \hat{h}_{n,c}^{t\top}) \otimes I \right) \text{Vec}(\hat{A}_{mn}^t) + 2\gamma (\hat{h}_{n,c}^t \otimes A_{mm}) \hat{h}_{m,a}^t.$$

We then define,

$$D_n^t = (I - 2\gamma \hat{h}_{n,c}^t \hat{h}_{n,c}^{t\top}) \otimes I, \quad B_{mn}^t = \hat{h}_{n,c}^t \otimes A_{mm}, \quad a_{mn}^t = \text{Vec}(\hat{A}_{mn}^t).$$

Then the vectorized update is given by,

$$a_{mn}^{t+1} = D_n^t a_{mn}^t + 2\gamma B_{mn}^t \hat{h}_{m,a}^t.$$

We wish to compute $\Sigma_{A_{mn}}^{t+1} = \text{Var}(a_{mn}^{t+1})$.

Using the property $\text{Var}[X + Z] = \text{Var}[X] + \text{Var}[Z] + \text{Cov}(X, Z) + \text{Cov}(Z, X)$ for any two vectors X , and Z .

We set, $X = D_n^t a_{mn}^t$, $Z = 2\gamma B_{mn}^t \hat{h}_{m,a}^t$. Then,

$$\Sigma_{A_{mn}}^{t+1} = \text{Var}[X] + \text{Var}[Z] + \text{Cov}(X, Z) + \text{Cov}(Z, X).$$

(1) *Variance of X:* D_n^t is deterministic, so

$$\text{Var}[X] = D_n^t \text{Var}(a_{mn}^t) D_n^{t\top} = D_n^t \Sigma_{A_{mn}}^t D_n^{t\top}.$$

(2) *Variance of Z:* $\hat{h}_{n,c}^t$ and A_{mm} are fixed at round t , hence

$$\text{Var}[Z] = 4\gamma^2 B_{mn}^t \text{Var}(\hat{h}_{m,a}^t) B_{mn}^{t\top} = 4\gamma^2 (\hat{h}_{n,c}^t \otimes A_{mm}) \Sigma_{h_m}^t (\hat{h}_{n,c}^t \otimes A_{mm})^\top.$$

(3) *Cross-covariance terms:* Since D_n^t and B_{mn}^t are deterministic,

$$\begin{aligned}\text{Cov}(X, Z) &= 2\gamma D_n^t \text{Cov}(a_{mn}^t, \hat{h}_{m,a}^t) B_{mn}^{t\top} = 2\gamma D_n^t \Gamma_{mn}^t B_{mn}^{t\top}, \\ \text{Cov}(Z, X) &= 2\gamma B_{mn}^t \text{Cov}(\hat{h}_{m,a}^t, a_{mn}^t) D_n^{t\top} = 2\gamma B_{mn}^t \Gamma_{mn}^{t\top} D_n^{t\top}.\end{aligned}$$

Adding the four contributions we obtain,

$$\begin{aligned}\Sigma_{A_{mn}}^{t+1} &= D_n^t \Sigma_{A_{mn}}^t D_n^{t\top} + 4\gamma^2 (\hat{h}_{n,c}^t \otimes A_{mm}) \Sigma_{h_m}^t (\hat{h}_{n,c}^t \otimes A_{mm})^\top \\ &\quad + 2\gamma (D_n^t \Gamma_{mn}^t B_{mn}^{t\top} + B_{mn}^t \Gamma_{mn}^{t\top} D_n^{t\top})\end{aligned}$$

□

K.8 Theorem 6.8

• **Theorem (Uncertainty Propagation within the Client)** *The client-parameter covariance $\Sigma_{\theta_m}^t$ obeys the following recursion: $\Sigma_{\theta_m}^t = H_m^{t-1} \Sigma_{\theta_m}^{t-1} H_m^{t-1\top} + G_m^{t-1} \Sigma_{h_m}^{t-1} G_m^{t-1\top} + (X_m + X_m^\top) - \sum_{n \neq m} (Y_{mn} + Y_{mn}^\top) - \sum_{n \neq m} (Z_{mn} + Z_{mn}^\top) + \sum_{n \neq m} P_m^{t-1} \Sigma_{A_{mn}}^{t-1} P_m^{t-1\top}$,*

where, $X_m = H_m^{t-1} \Lambda_m^{t-1} G_m^{t-1\top}$, $Y_{mn} = H_m^{t-1} \Psi_{mn}^{t-1} P_m^{t-1\top}$, $Z_{mn} = G_m^{t-1} \Gamma_{mn}^{t-1} P_m^{t-1\top}$, and, $G_m^{t-1} := 2\eta_1 (y_m^{t-1} \otimes (C_{mm} A_{mm})^\top)$, $P_m^{t-1} := -2\eta_2 (y_m^{t-1} \otimes A_{mm}^\top)$, $H_m^{t-1} := I_{p_m d_m} - 2\eta_1 (y_m^{t-1} y_m^{t-1\top}) \otimes ((C_{mm} A_{mm})^\top C_{mm} A_{mm}) - 2\eta_2 (y_m^{t-1} y_m^{t-1\top}) \otimes (A_{mm}^\top A_{mm})$

Proof. All random variables, distributional assumptions (A1–A6) and second-moment symbols $\Sigma_{\theta_m}^t, \Sigma_{h_m}^t, \Sigma_{A_{mn}}^t, \Lambda_m^t, \Psi_{mn}^t, \Gamma_{mn}^t, \Omega_m^t$ are defined in Section 5.

Computing the analytical values of $\nabla_{\theta_m^t} (L_m)_a$, and $\nabla_{\theta_m^t} L_s$, and substituting them in Eq (5) of Section 3.1, we have the following client model update (for the FedGC framework):

$$\theta_m^t = \theta_m^{t-1} + 2\eta_1 (C_{mm} A_{mm})^\top \left(y_m^{t-1} - C_{mm} A_{mm} \hat{h}_{m,c}^{t-1} \right) y_m^{t-1\top} - 2\eta_2 A_{mm}^\top \left(\sum_{n \neq m} A_{mn}^{t-1} \hat{h}_{n,c}^{t-1} \right) y_m^{t-1\top}.$$

Let $v_m^t := \text{Vec}(\theta_m^t)$. Using the property $\text{Vec}(AXB) = (B^\top \otimes A) \text{Vec}(X)$ and $\text{Vec}(A \hat{h}) = (\hat{h}^\top \otimes I) \text{Vec}(A)$ for any matrices A, B, X and vector \hat{h} , we obtain the following:

$$v_m^t = H_m^{t-1} v_m^{t-1} + G_m^{t-1} \hat{h}_{m,a}^{t-1} + P_m^{t-1} \sum_{n \neq m} a_{mn}^{t-1} + u_m^{t-1},$$

where these matrices (H_m^t, G_m^t, P_m^t) are exactly those stated in the theorem. We define $u_m^{t-1} := 2\eta_1 (y_m^{t-1} \otimes (C_{mm} A_{mm})^\top) (y_m^{t-1} - C_{mm} A_{mm} \hat{h}_{m,c}^{t-1})$. By assumption (A4) u_m^{t-1} has mean 0 and vanishing covariance: $\mathbb{E}[u_m^{t-1}] = 0$, $\text{Var}(u_m^{t-1}) = 0$.

First, we have the following:

$$\text{Var}(H_m^{t-1} v_m^{t-1}) = H_m^{t-1} \Sigma_{\theta_m}^{t-1} H_m^{t-1\top}, \quad \text{Var}(G_m^{t-1} \hat{h}_{m,a}^{t-1}) = G_m^{t-1} \Sigma_{h_m}^{t-1} G_m^{t-1\top}.$$

We also denote $S_m^{t-1} := \sum_{n \neq m} a_{mn}^{t-1}$. Independence of different off-diagonal blocks a_{mn}^{t-1} in assumption (A2) yields $\text{Var}(S_m^{t-1}) = \sum_{n \neq m} \Sigma_{A_{mn}}^{t-1}$; hence

$$\text{Var}(P_m^{t-1} S_m^{t-1}) = \sum_{n \neq m} P_m^{t-1} \Sigma_{A_{mn}}^{t-1} P_m^{t-1\top}.$$

Independence assumptions (A2) imply that cross terms with different client indices cancel. The only non-zero covariances are

$$\begin{aligned}\text{Cov}(Hv, G\hat{h}) &= H_m^{t-1} \Lambda_m^{t-1} G_m^{t-1\top} = X_m, \\ \text{Cov}(Hv, PS) &= \sum_{n \neq m} H_m^{t-1} \Psi_{mn}^{t-1} P_m^{t-1\top} = \sum_{n \neq m} Y_{mn}, \\ \text{Cov}(G\hat{h}, PS) &= \sum_{n \neq m} G_m^{t-1} \Gamma_{mn}^{t-1} P_m^{t-1\top} = \sum_{n \neq m} Z_{mn}.\end{aligned}$$

Each term X_m, Y_{mn}, Z_{mn} appears together with its transpose in the variance expansion. Applying $\text{Var}(\cdot)$ to $\text{Vec}(\theta_m)$, and using $\text{Var}(u_m^{t-1}) = 0$, we obtain:

$$\begin{aligned}\Sigma_{\theta_m}^t &= H_m^{t-1} \Sigma_{\theta_m}^{t-1} H_m^{t-1\top} + G_m^{t-1} \Sigma_{h_m}^{t-1} G_m^{t-1\top} + (X_m + X_m^\top) \\ &\quad - \sum_{n \neq m} (Y_{mn} + Y_{mn}^\top) - \sum_{n \neq m} (Z_{mn} + Z_{mn}^\top) + \sum_{n \neq m} P_m^{t-1} \Sigma_{A_{mn}}^{t-1} P_m^{t-1\top}.\end{aligned}$$

□

K.9 Proposition 7.1

• **Proposition (Gain Matrices Convergence)** *Under the above assumptions, the gain matrices used in Section 6 converges as, $\lim_{t \rightarrow \infty} (D_n^t, H_m^t, G_m^t, P_m^t) = (D_n, H_m, G_m, P_m)$ where, $D_n = (I - 2\gamma \hat{h}_{n,c} \hat{h}_{n,c}^\top) \otimes I$, $G_m = 2\eta_1 (\mu_{y_m} \otimes (C_{mm} A_{mm})^\top)$, $P_m = -2\eta_2 (\mu_{y_m} \otimes A_{mm}^\top)$ and $H_m = I_{p_m d_m} - 2\eta_1 (\mu_{y_m} \mu_{y_m}^\top) \otimes ((C_{mm} A_{mm})^\top C_{mm} A_{mm}) - 2\eta_2 (\mu_{y_m} \mu_{y_m}^\top) \otimes (A_{mm}^\top A_{mm})$.*

Proof. We prove the convergence of the gain matrices under the assumptions (provided in Section 7):

(I) $\lim_{t \rightarrow \infty} y_m^t = \mu_{y_m}$ (client data converges)

(II) $\lim_{t \rightarrow \infty} \hat{h}_{m,c}^t = \hat{h}_{m,c}$ (client state estimates converge)

First, for $D_n^t = (I - 2\gamma \hat{h}_{n,c}^t \hat{h}_{n,c}^{t\top}) \otimes I$ we have,

$$\begin{aligned}\lim_{t \rightarrow \infty} D_n^t &= \left(I - 2\gamma \left(\lim_{t \rightarrow \infty} \hat{h}_{n,c}^t \right) \left(\lim_{t \rightarrow \infty} \hat{h}_{n,c}^t \right)^\top \right) \otimes I \\ &= (I - 2\gamma \hat{h}_{n,c} \hat{h}_{n,c}^\top) \otimes I =: D_n\end{aligned}$$

Next for $G_m^t = 2\eta_1 (y_m^t \otimes (C_{mm} A_{mm})^\top)$ we have,

$$\begin{aligned}\lim_{t \rightarrow \infty} G_m^t &= 2\eta_1 \left(\left(\lim_{t \rightarrow \infty} y_m^t \right) \otimes (C_{mm} A_{mm})^\top \right) \\ &= 2\eta_1 (\mu_{y_m} \otimes (C_{mm} A_{mm})^\top) =: G_m\end{aligned}$$

Similarly for $P_m^t = -2\eta_2 (y_m^t \otimes A_{mm}^\top)$ we have,

$$\begin{aligned}\lim_{t \rightarrow \infty} P_m^t &= -2\eta_2 \left(\left(\lim_{t \rightarrow \infty} y_m^t \right) \otimes A_{mm}^\top \right) \\ &= -2\eta_2 (\mu_{y_m} \otimes A_{mm}^\top) =: P_m\end{aligned}$$

Finally for H_m^t we have,

$$\begin{aligned}\lim_{t \rightarrow \infty} H_m^t &= I_{p_m d_m} - 2\eta_1 \left(\left(\lim_{t \rightarrow \infty} y_m^t y_m^{t\top} \right) \otimes ((C_{mm} A_{mm})^\top C_{mm} A_{mm}) \right) \\ &\quad - 2\eta_2 \left(\left(\lim_{t \rightarrow \infty} y_m^t y_m^{t\top} \right) \otimes (A_{mm}^\top A_{mm}) \right)\end{aligned}$$

Using the fact that $\lim_{t \rightarrow \infty} y_m^t y_m^{t\top} = \mu_{y_m} \mu_{y_m}^\top + \Sigma_{y_m}$ (from the stationary distribution), but under Assumption (A4) that Σ_{y_m} is constant, we get,

$$\begin{aligned}H_m &= I_{p_m d_m} - 2\eta_1 (\mu_{y_m} \mu_{y_m}^\top \otimes (C_{mm} A_{mm})^\top C_{mm} A_{mm}) \\ &\quad - 2\eta_2 (\mu_{y_m} \mu_{y_m}^\top \otimes A_{mm}^\top A_{mm})\end{aligned}$$

□

K.10 Proposition 7.2

• **Proposition** If $\rho(D_n) < 1$ and $\rho(H_m) < 1$ then we have, $\lim_{t \rightarrow \infty} (\Gamma_{mn}^t, \Psi_{mn}^t) = (\Gamma_{mn}^\infty, \Psi_{mn}^\infty)$ with $\Gamma_{mn}^\infty = (I - D_n)^{-1} 2\gamma B_{mn} \Sigma_{h_m}^\infty$, & $\Psi_{mn}^\infty = (I - H_m \otimes D_n)^{-1} \text{Vec}(D_n \Gamma_{mn}^\infty G_m^\top - D_n \Sigma_{A_{mn}}^\infty P_m^\top)$.

Proof. Convergence of Γ_{mn}^t : From Lemma 6.3, we have the recursion as follows,

$$\Gamma_{mn}^{t+1} = D_n^t \Gamma_{mn}^t + 2\gamma B_{mn}^t \Sigma_{h_m}^t$$

Taking limits $t \rightarrow \infty$ and using Proposition 7.1 we obtain,

$$\begin{aligned} \Gamma_{mn}^\infty &= D_n \Gamma_{mn}^\infty + 2\gamma B_{mn} \Sigma_{h_m}^\infty \\ (I - D_n) \Gamma_{mn}^\infty &= 2\gamma B_{mn} \Sigma_{h_m}^\infty \end{aligned}$$

Since $\rho(D_n) < 1$, the matrix $(I - D_n)$ is invertible, giving:

$$\Gamma_{mn}^\infty = (I - D_n)^{-1} 2\gamma B_{mn} \Sigma_{h_m}^\infty$$

Convergence of Ψ_{mn}^t : From Lemma 6.4, the recursion is given by,

$$\begin{aligned} \Psi_{mn}^{t+1} &= D_n^t \Psi_{mn}^t H_m^{t\top} + D_n^t \Gamma_{mn}^t G_m^{t\top} - D_n^t \Sigma_{A_{mn}}^t P_m^{t\top} \\ &\quad + 2\gamma B_{mn}^t \Lambda_m^t H_m^{t\top} + 2\gamma B_{mn}^t \Sigma_{h_m}^t G_m^{t\top} - 2\gamma B_{mn}^t \Gamma_{mn}^{t\top} P_m^{t\top} \end{aligned}$$

At steady-state, using Proposition 7.1 we obtain,

$$\begin{aligned} \Psi_{mn}^\infty &= D_n \Psi_{mn}^\infty H_m^\top + D_n \Gamma_{mn}^\infty G_m^\top - D_n \Sigma_{A_{mn}}^\infty P_m^\top \\ &\quad + 2\gamma B_{mn} \Lambda_m^\infty H_m^\top + 2\gamma B_{mn} \Sigma_{h_m}^\infty G_m^\top - 2\gamma B_{mn} \Gamma_{mn}^{\infty\top} P_m^\top \end{aligned}$$

This can be rewritten as a vectorized equation using $\text{Vec}(\cdot)$,

$$\text{Vec}(\Psi_{mn}^\infty) = (H_m \otimes D_n) \text{Vec}(\Psi_{mn}^\infty) + \text{Vec}(X)$$

where X collects all remaining terms.

Since $\rho(H_m \otimes D_n) = \rho(H_m) \rho(D_n) < 1$ by assumption, we have,

$$\text{Vec}(\Psi_{mn}^\infty) = (I - H_m \otimes D_n)^{-1} \text{Vec}(X)$$

Substituting back X we obtain,

$$\Psi_{mn}^\infty = (I - H_m \otimes D_n)^{-1} \text{Vec}(D_n \Gamma_{mn}^\infty G_m^\top - D_n \Sigma_{A_{mn}}^\infty P_m^\top)$$

□

K.11 Corollary 7.3

• **Corollary** The above assumptions lead to convergence of the uncertainty of the client states $\Sigma_{h_m}^t$ as follows: $\lim_{t \rightarrow \infty} \Sigma_{h_m}^t := \Sigma_{h_m}^\infty = \kappa_m \Sigma_{\theta_m}^\infty + \Omega_m^\infty (\mu_{y_m} \otimes I)^\top + (\mu_{y_m} \otimes I) \Omega_m^{\infty\top}$, where $\kappa_m = \text{tr}(\Sigma_{y_m}) + \|\mu_{y_m}\|^2$ and $\Omega_m^\infty = \Sigma_{\theta_m}^\infty \mu_{y_m}$.

Proof. From Lemma 6.5, the client state variance evolves as follows,

$$\Sigma_{h_m}^t = \kappa_m^t \Sigma_{\theta_m}^t + \Omega_m^t (\mu_{y_m}^t \otimes I_{p_m})^\top + (\mu_{y_m}^t \otimes I_{p_m}) \Omega_m^{t\top}$$

where $\kappa_m^t = \text{tr}(\Sigma_{y_m}^t) + \|\mu_{y_m}^t\|^2$.

Under the stationarity Assumption (A4) and Proposition 7.1 we define the following,

$$\begin{aligned} \Sigma_{\theta_m}^\infty &:= \lim_{t \rightarrow \infty} \Sigma_{\theta_m}^t \\ \Omega_m^\infty &:= \lim_{t \rightarrow \infty} \Omega_m^t \\ \kappa_m &:= \lim_{t \rightarrow \infty} \kappa_m^t = \text{tr}(\Sigma_{y_m}) + \|\mu_{y_m}\|^2 \end{aligned}$$

From Proposition 6.1 and the steady-state analysis we have,

$$\Omega_m^\infty = \text{Cov}(v_m^\infty, y_m) = \Sigma_{\theta_m}^\infty \mu_{y_m}$$

since at steady-state, the parameter covariance dominates the data-model correlation.

Substituting these limits into the variance expression, we obtain,

$$\begin{aligned} \Sigma_{h_m}^\infty &= \kappa_m \Sigma_{\theta_m}^\infty + \Sigma_{\theta_m}^\infty \mu_{y_m} (\mu_{y_m} \otimes I_{p_m})^\top + (\mu_{y_m} \otimes I_{p_m}) \mu_{y_m}^\top \Sigma_{\theta_m}^\infty \\ &= \kappa_m \Sigma_{\theta_m}^\infty + \Sigma_{\theta_m}^\infty (\mu_{y_m} \mu_{y_m}^\top \otimes I_{p_m}) + (\mu_{y_m} \mu_{y_m}^\top \otimes I_{p_m}) \Sigma_{\theta_m}^\infty \end{aligned}$$

Simplifying using the Kronecker product properties, we have,

$$\lim_{t \rightarrow \infty} \Sigma_{h_m}^t = \kappa_m \Sigma_{\theta_m}^\infty + \Omega_m^\infty (\mu_{y_m} \otimes I_{p_m})^\top + (\mu_{y_m} \otimes I_{p_m}) \Omega_m^{\infty \top}$$

with $\Omega_m^\infty = \Sigma_{\theta_m}^\infty \mu_{y_m}$. □

K.12 Theorem 7.4

• **Theorem (Convergence of Server Model's Uncertainty)** Let $\rho(D_n) < 1$. Define the linear map $\mathcal{L}_n(X) = D_n X D_n^\top$ and the injection $Q_{mn}(\Sigma) = 4\gamma^2 B_{mn} (\kappa_m \Sigma + \Sigma M_m M_m^\top + M_m M_m^\top \Sigma) B_{mn}^\top$. Then, $\Sigma_{A_{mn}}^\infty := \lim_{t \rightarrow \infty} \Sigma_{A_{mn}}^t$ exists, is unique, and is given by, $\Sigma_{A_{mn}}^\infty = \sum_{k=0}^\infty \mathcal{L}_n^k(Q_{mn}(\Sigma_{\theta_m}^\infty))$

Proof. From Theorem 6.7, the server parameter covariance evolves as follows,

$$\begin{aligned} \Sigma_{A_{mn}}^{t+1} &= D_n^t \Sigma_{A_{mn}}^t D_n^{t\top} + 4\gamma^2 B_{mn}^t \Sigma_{h_m}^t B_{mn}^{t\top} \\ &\quad + 2\gamma (D_n^t \Gamma_{mn}^t B_{mn}^{t\top} + B_{mn}^t \Gamma_{mn}^{t\top} D_n^{t\top}) \end{aligned}$$

Taking limits $t \rightarrow \infty$ and using Proposition 7.1 we have,

$$\begin{aligned} \Sigma_{A_{mn}}^\infty &= D_n \Sigma_{A_{mn}}^\infty D_n^\top + 4\gamma^2 B_{mn} \Sigma_{h_m}^\infty B_{mn}^\top \\ &\quad + 2\gamma (D_n \Gamma_{mn}^\infty B_{mn}^\top + B_{mn} \Gamma_{mn}^{\infty \top} D_n^\top) \end{aligned}$$

From Corollary 7.3, we substitute $\Sigma_{h_m}^\infty$ as follows,

$$\Sigma_{h_m}^\infty = \kappa_m \Sigma_{\theta_m}^\infty + \Sigma_{\theta_m}^\infty M_m M_m^\top + M_m M_m^\top \Sigma_{\theta_m}^\infty$$

where $M_m = \mu_{y_m} \otimes I_{p_m}$ and $\kappa_m = \text{tr}(\Sigma_{y_m}) + \|\mu_{y_m}\|^2$.

Defining the linear operator $\mathcal{L}_n(X) = D_n X D_n^\top$ and the quadratic form we have,

$$Q_{mn}(\Sigma) = 4\gamma^2 B_{mn} (\kappa_m \Sigma + \Sigma M_m M_m^\top + M_m M_m^\top \Sigma) B_{mn}^\top$$

The steady-state equation thus becomes,

$$\Sigma_{A_{mn}}^\infty = \mathcal{L}_n(\Sigma_{A_{mn}}^\infty) + Q_{mn}(\Sigma_{\theta_m}^\infty)$$

Since $\rho(D_n) < 1$ (given as a condition), the operator $\mathcal{L}_n(\cdot)$ is a contraction, and the solution is given by the Neumann series:

$$\Sigma_{A_{mn}}^\infty = \sum_{k=0}^\infty \mathcal{L}_n^k(Q_{mn}(\Sigma_{\theta_m}^\infty))$$

With I being the identity operator, the above expression can be re-written as,

$$(I - \mathcal{L}_n)(\Sigma_{A_{mn}}^\infty) = Q_{mn}$$

This has a formal solution with operator inversion such that,

$$\Sigma_{A_{mn}}^\infty = (I - \mathcal{L}_n)^{-1} Q_{mn}$$

Since $\rho(D_n) < 1$, the Neumann series expansion is valid thus we can use,

$$(I - \mathcal{L}_n)^{-1} = \sum_{k=0}^\infty \mathcal{L}_n^k$$

Substituting this into the equation for $\Sigma_{A_{mn}}^\infty$ we obtain,

$$\Sigma_{A_{mn}}^\infty = \sum_{k=0}^{\infty} \mathcal{L}_n^k(Q_{mn})$$

The series converges because $\|\mathcal{L}_n^k(Q_{mn})\| \leq \rho(D_n)^{2k} \|Q_{mn}\| \rightarrow 0$ as $k \rightarrow \infty$. Uniqueness follows from the Banach fixed-point theorem, as \mathcal{L}_n is a contraction mapping on the space of positive semidefinite matrices with a matrix norm. \square

K.13 Theorem 7.5

• **Theorem (Convergence of Client Model’s Uncertainty)** Let $\rho(H_m) < 1$. Write $\mathcal{M}_m(\Sigma) = H_m \Sigma H_m^\top$ and $R_m(\Sigma) = G_m (\kappa_m \Sigma + \Sigma M_m M_m^\top + M_m M_m^\top \Sigma) G_m^\top$. Then the steady-state $\Sigma_{\theta_m}^\infty := \lim_{t \rightarrow \infty} \Sigma_{\theta_m}^t$ is the unique solution to $\Sigma_{\theta_m}^\infty = \mathcal{M}_m(\Sigma_{\theta_m}^\infty) + R_m(\Sigma_{\theta_m}^\infty) + P_m \Sigma_{A_{mn}}^\infty P_m^\top$.

Proof. From Theorem 6.8, the client parameter covariance evolves as follows,

$$\Sigma_{\theta_m}^{t+1} = H_m^t \Sigma_{\theta_m}^t H_m^{t\top} + R_m^t(\Sigma_{\theta_m}^t) + P_m^t \Sigma_{A_{mn}}^t P_m^{t\top} + \text{cross terms}$$

where R_m^t collects terms quadratic in $\Sigma_{\theta_m}^t$.

Under Proposition 7.1’s convergence and Theorem 7.4’s steady-state for $\Sigma_{A_{mn}}^\infty$, we take limits as,

$$\Sigma_{\theta_m}^\infty = H_m \Sigma_{\theta_m}^\infty H_m^\top + R_m(\Sigma_{\theta_m}^\infty) + P_m \Sigma_{A_{mn}}^\infty P_m^\top$$

The quadratic term R_m derives from Corollary 7.3’s expression as,

$$R_m(\Sigma) = G_m (\kappa_m \Sigma + \Sigma M_m M_m^\top + M_m M_m^\top \Sigma) G_m^\top$$

with $G_m = 2\eta_1 (\mu_{y_m} \otimes (C_{mm} A_{mm})^\top)$ and $M_m = \mu_{y_m} \otimes I_{p_m}$.

Rewriting the fixed-point equation using the linear operator $\mathcal{M}_m(X) = H_m X H_m^\top$ we obtain,

$$\Sigma_{\theta_m}^\infty = \mathcal{M}_m(\Sigma_{\theta_m}^\infty) + R_m(\Sigma_{\theta_m}^\infty) + P_m \Sigma_{A_{mn}}^\infty P_m^\top$$

Since $\rho(H_m) < 1$ (given), \mathcal{M}_m is a contraction, guaranteeing a unique solution. \square

L Limitations

Our theoretical analysis is derived under a linear time-invariant state-space model with Gaussian noise. In particular, the closed-form covariance recursions, spectral-radius-based convergence conditions, and the asymptotic independence from epistemic priors rely on this setting. Although Appendix J discusses extensions to certain nonlinear models using EKF- and GP-based approximations, these extensions preserve only the structural form of the recursions. We do not establish convergence guarantees, fixed-point uniqueness, or aleatoric-only steady-state behavior in the nonlinear regime. A rigorous nonlinear treatment is left to future work.

Assumption (A2) requires the server parameters A_{mn}^t to be mutually independent across block-rows. This assumption eliminates cross-block covariance terms and enables the block-wise decomposition used throughout the analysis. In practical systems, however, shared latent confounders or correlated process noise across subsystems may violate this assumption. In such settings, the off-diagonal cross-block covariances must be propagated explicitly, increasing the recursion complexity from $\mathcal{O}(M)$ to $\mathcal{O}(M^2)$. Characterizing uncertainty propagation under correlated subsystem dynamics remains an open problem.

Finally, the asymptotic result that epistemic uncertainty vanishes and steady-state uncertainty depends only on aleatoric quantities assumes full convergence of the contraction maps \mathcal{L}_n and \mathcal{M}_m . However, the post-training hypothesis test in Section 7 is applied at finite training horizons, where residual epistemic uncertainty may still persist. Consequently, the asymptotic covariance $\Sigma_{A_{mn}}^\infty$ may not perfectly capture the finite-time uncertainty, potentially affecting the Type-I and Type-II error rates of the test. We do not derive finite-sample bounds quantifying the gap between $\Sigma_{A_{mn}}^t$ and $\Sigma_{A_{mn}}^\infty$, nor corresponding corrections to the hypothesis test.